Title Page

Pharmacology of a central nervous system delivered 2'-*O*-methoxyethyl-modified survival of motor neuron splicing oligonucleotide in mice and non-human primates

Frank Rigo, Seung J. Chun, Daniel A. Norris, Gene Hung, Sam Lee, John Matson, Robert A. Fey, Hans Gaus, Yimin Hua, John S. Grundy, Adrian R. Krainer, Scott P. Henry and C. Frank Bennett

ISIS Pharmaceuticals, Carlsbad, California, USA (F.R., S.J.C., D.A.N., G.H., S.L., J.M., R.A.F., H.G., J.S.G., S.P.H., C.F.B.); and Cold Spring Harbor Laboratory, Cold Spring Harbor, New York, USA (Y.H., A.R.K.)

JPET Fast Forward. Published on April 30, 2014 as DOI: 10.1124/jpet.113.212407
This article has not been copyedited and formatted. The final version may differ from this version.

Running Title Page

Running title: Pharmacology of ISIS 396443 in the central nervous system

Corresponding author:

Frank Rigo

2855 Gazelle Court

Carlsbad, CA 92010

USA

Email: frigo@isisph.com

Number of text pages: 35

Number of tables: 0

Number of figures: 4

Number of references: 54

Number of words in Abstract: 191

Number of words in Introduction: 678

Number of words in Discussion: 892

Abbreviations:

2'-MOE, 2'-*O*-methoxyethyl

2'-OMe, 2'-*O*-methyl

ALT, alanine aminotransferase

ASO, antisense oligonucleotide

JPET Fast Forward. Published on April 30, 2014 as DOI: 10.1124/jpet.113.212407
This article has not been copyedited and formatted. The final version may differ from this version.

AST, aspartate aminotransferase

BUN, blood urea nitrogen

cEt, 2',4'-constrained 2'-*O*-ethyl

CGE-UV, capillary gel electrophoresis coupled with UV detection

CNS, central nervous system

CSF, cerebrospinal fluid

HELISA, hybridization-based enzyme-linked immunosorbent assay

HPLC-MS/MS, high performance liquid chromatography coupled with tandem mass spectrometry detection

HPLC-UV, high performance liquid chromatography coupled with ultraviolet detection

ICV, intracerebroventricular

IHC, immunohistochemistry

IP, intraperitoneal

LNA, locked nucleic acid

LP, lumbar puncture

NBF, neutral buffered formalin

NHP, non-human primate

PD, pharmacodynamic

PK, pharmacokinetic

PMO, phosphorodiamindate morpholino

SMA, spinal muscular atrophy

SMN, survival of motor neuron

UV, ultraviolet

JPET Fast Forward. Published on April 30, 2014 as DOI: 10.1124/jpet.113.212407
This article has not been copyedited and formatted. The final version may differ from this version.

Recommended section assignment: Drug Discovery and Translational Medicine

JPET Fast Forward. Published on April 30, 2014 as DOI: 10.1124/jpet.113.212407
This article has not been copyedited and formatted. The final version may differ from this version.

Abstract

Spinal muscular atrophy (SMA) is a debilitating neuromuscular disease caused by the loss of survival of motor neuron (SMN) protein. Previously we demonstrated that ISIS 396443, an antisense oligonucleotide (ASO) targeted to the *SMN2* pre-mRNA, is a potent inducer of *SMN2* exon 7 inclusion and SMN protein expression, and improves function and survival of mild and severe SMA mouse models. Here we demonstrate that ISIS 396443 is the most potent ASO in central nervous system (CNS) tissues of adult mice, compared to several other chemically modified ASOs. We evaluated methods of ISIS 396443 delivery to the CNS and characterized its pharmacokinetics and pharmacodynamics in rodents and non-human primates (NHPs). Intracerebroventricular (ICV) bolus injection is a more efficient method of delivering ISIS 396443 to the CNS of rodents, compared to ICV infusion. For both methods of delivery, the duration of ISIS-396443-mediated *SMN2* splicing correction is long-lasting, with maximal effects still observed 6 months after treatment discontinuation. Administration of ISIS 396443 to the CNS of NHPs by a single intrathecal bolus injection results in widespread distribution throughout the spinal cord. Based upon these preclinical studies, we have advanced ISIS 396443 into clinical development.

JPET Fast Forward. Published on April 30, 2014 as DOI: 10.1124/jpet.113.212407
This article has not been copyedited and formatted. The final version may differ from this version.

Introduction

In its most severe form, spinal muscular atrophy (SMA) is the leading genetic cause of infant mortality (Lunn and Wang, 2008). The disease manifests as a neuromuscular disorder with severe muscle weakness and atrophy of the voluntary muscles of the limbs and trunk, with eventual paralysis as a result of the degeneration of motor neurons in the anterior horn of the spinal cord (Crawford and Pardo, 1996). The genetic basis of SMA is the loss of function of the survival motor neuron (SMN) protein caused by deletion or, more rarely, by mutations in the *SMN1* gene (Lefebvre et al., 1995). Even though no consensus has emerged on how the reduction in levels of SMN protein causes disease, it is widely believed that a recovery in the levels of SMN protein should provide a therapeutic benefit (Burghes and Beattie, 2009).

The primary modifier of SMA is the *SMN2* gene, a paralog of *SMN1*. In humans, *SMN2* is often present in multiple copies and patients who have a greater number of copies usually have a less severe form of the disease (Feldkotter et al., 2002; Prior et al., 2004). This is because the *SMN2* gene expresses a small amount of SMN protein due to a mutation in exon 7 that augments its alternative splicing (Coovert et al., 1997; Lefebvre et al., 1997; Lorson et al., 1999; Monani et al., 1999). Omission of exon 7 results in the production of a protein truncated at the C-terminus that is unstable and rapidly degraded (Cho and Dreyfuss, 2010). Therefore, the gene-dosage effect arises because a greater number of *SMN2* copies results in a larger amount of full-length SMN protein produced (Monani et al., 2000).

Numerous approaches have been developed to increase the levels of SMN protein. These include: small molecules to augment *SMN2* transcription, correct *SMN2* splicing, cause translational read-through and stabilize *SMN2* transcripts (Lunn and Wang, 2008); SMN gene delivery to replace SMN protein (Foust et al., 2010; Passini et al., 2010); antisense

oligonucleotide (ASO) based approaches to correct *SMN2* splicing (Lim and Hertel, 2001; Miyajima et al., 2002; Cartegni and Krainer, 2003; Skordis et al., 2003; Singh et al., 2006; Hua et al., 2007; Dickson et al., 2008; Hua et al., 2008; Williams et al., 2009; Hua et al., 2011; Porensky et al., 2011; Osman et al., 2012; Mitrpant et al., 2013; Zhou et al., 2013); and antisense-producing vector-based strategies (Geib and Hertel, 2009; Meyer et al., 2009) including trans-splicing (Coady et al., 2007; Coady and Lorson, 2010). Some of these strategies have not yet been tested in animal models of SMA, but others have already been shown to be beneficial (Bebee et al., 2012).

ISIS 396443 (also known as ISIS-SMN_{Rx}, and previously referred to as ASO-10-27) targets a site in intron 7, termed ISS-N1, that was previously shown to repress *SMN2* exon 7 inclusion (Singh et al., 2006). Hybridization of ISIS 396443 to ISS-N1 prevents the recruitment of the splicing repressor heterogeneous nuclear ribonucleoprotein A1 and A2 (hnRNPA1/A2) and results in almost complete *SMN2* exon 7 inclusion in cell culture (Hua et al., 2008; Rigo et al., 2012). Robust splicing correction and SMN protein production is also observed in the CNS of mice transgenic for *SMN2* after central administration of ISIS 396443 (Hua et al., 2010). In addition, in two severe SMA mouse models, central administration of the ASO delays the loss of motor neurons, preserves neuromuscular junctions, improves muscle physiology, and increases survival (Hua et al., 2011; Passini et al., 2011). Remarkably, peripheral administration of ISIS 396443 shows a much more profound improvement in survival, in line with mounting evidence indicating that the severe SMA mouse models have significant peripheral defects (Hamilton and Gillingwater, 2013).

Here we have expanded the pre-clinical characterization of ISIS 396443. We compared ISIS 396443 to several other chemically modified ASOs in order to identify the most potent ASO for

JPET Fast Forward. Published on April 30, 2014 as DOI: 10.1124/jpet.113.212407
This article has not been copyedited and formatted. The final version may differ from this version.

SMN2 splicing correction in the CNS of adult rodents. We also assessed methods of delivering ISIS 396443 to the CNS, and characterized its pharmacokinetic (PK) and pharmacodynamic (PD) properties in rodents and non-human primates (NHPs).

JPET Fast Forward. Published on April 30, 2014 as DOI: 10.1124/jpet.113.212407
This article has not been copyedited and formatted. The final version may differ from this version.

Materials and Methods

Oligonucleotides. Synthesis and purification of all chemically modified oligonucleotides were performed as previously described (Swayze et al., 2007). For chemically modified oligonucleotides, see Supplemental Table 1, and for DNA primers, see Supplemental Table 2.

Dosing of mice. All protocols met ethical standards for animal experimentation and were approved by the Institutional Animal Care and Use Committee (IACUC). Adult male and female SMA type III mice ($Smn1^{-/-}$; $SMN2^{+/+}$) were obtained from Jackson Laboratory (FVB.Cg-Tg(SMN2)2HungSMN1tm1Hung/J, stock number 005058). The lyophilized ASOs were dissolved in sterile PBS without calcium or magnesium and quantified by ultraviolet (UV) spectrometry. The ASOs were then diluted to the desired concentration required for dosing mice and sterilized through a 0.2 µm filter. ICV infusions (Hua and Krainer, 2012) and IP bolus injections (Rigo et al., 2012) were performed as previously described. For ICV bolus injections, mice were placed in a stereotaxic frame and anesthetized with 2 % isofluorane by a nose cone fitted into the frame. The scalp and anterior back was then shaved and disinfected. A 1-1.5 cm incision was made in the scalp and the subcutaneous tissue and periosteum was scraped from the skull with a sterile cotton-tipped applicator. A 10 µl Hamilton micro syringe with a 26 G Huber point removable needle was used to punch through the skull at 0.2 mm posterior and 1.0 mm lateral to the bregma, and lowered to a depth of 3 mm. 5 µl of ASO solution was injected a single time into the right lateral ventricle at a rate of 1 µl/s. After 5 min, the needle was slowly withdrawn and the incision was sutured. The mice were then allowed to recover from the anesthesia in their home cage.

Dosing of non-human primates. NHP studies were performed at the Northern Biomedical Research (Muskegon, MI), and were approved by the Institutional Animal Care and Use

JPET Fast Forward. Published on April 30, 2014 as DOI: 10.1124/jpet.113.212407
This article has not been copyedited and formatted. The final version may differ from this version.

Committee (IACUC). Male and female cynomolgus monkeys weighing 2 to 5 kg were anesthetized and implanted with intrathecal indwelling catheters. The monkeys were allowed to recover from the implantation surgery for several days. 100 mg/ml solutions of ASO were diluted to the desired final concentration in artificial CSF. Monkeys received ASO in a single 1 ml IT bolus injection that lasted 3 min. Tissues were collected for analysis 7 days after the injection.

RT-PCR. For spinal cord, a 2 mm lumbar section was collected. For brain, a 1 mm coronal section, 2 mm posterior to the injection site, was collected. For liver, a 3 mm^3 punch was collected. Each piece of tissue was homogenized in a 2 ml tube containing Lysing Matrix D (MP Biomedicals), 500 µl RLT buffer (Qiagen) and 1% (v/v) β-mercaptoethanol. Homogenization was performed for 20 s at 6,000 r.p.m. using a FastPrep Automated Homogenizer (MP Biomedicals). 10 µl of lysate was used to isolate RNA with an RNeasy 96 Kit (Qiagen) that included in-column DNA digestion with 50 U of DNase I (Invitrogen). Real-time RT-PCR was performed as previously described (Rigo et al., 2012). For Supplemental Fig. 11, RNA was isolated with an RNeasy 96 Kit (Qiagen) that included in-column DNA digestion with 30 U of DNase I (Invitrogen). Real-time RT-PCR was performed as previously described (Rigo et al., 2012). The FL or Δ7 *SMN2* expression level was normalized to either that of *Gapdh* or total *SMN2*, and this was further normalized to the level in PBS-treated mice or untreated cells. For the analysis of *Aif1* expression, normalization was to the levels of *Gapdh*. For Supplemental Figs. 9A and 17, RNA was isolated with an RNeasy Mini Kit (Qiagen). In-column DNA digestion was done with 50 U of DNase I (Invitrogen). For Supplemental Fig. 9A, radioactive RT-PCR was performed as previously described (Hua and Krainer, 2012). For Supplemental Fig. 17, 500 ng of RNA was reverse-transcribed using oligo(dT) as the primer and SuperScript II

reverse transcriptase (Invitrogen). PCR was performed with Platinum Taq DNA polymerase (Invitrogen). Amplification was for 30 cycles (94 °C for 30 s, 55 °C for 30 s and 72 °C for 36 s). All PCR products were separated by agarose gel electrophoresis and stained with ethidium bromide.

Quantification of ASO tissue concentration. For rodents, a 1 mm brain coronal section, 3 mm posterior to the injection site and the thoracic spinal cord were collected for bioanalytical evaluation. A 2 mm coronal brain section immediately posterior to the injection site and a 2 mm cervical spinal cord section were preserved in 10 % neutral buffered formalin (NBF) for immunostaining as described below. For non-human primates, the brain was sectioned in a brain matrix at 3 mm coronal slice thickness. The first slice and every other slice were frozen for bioanalytical evaluation. The interleaved brain slices were preserved in 10 % NBF for immunostaining. The spinal cord was divided into lumbar, thoracic, and cervical sections and a 1 cm portion of the rostral end of each was frozen for bioanalytical analysis. The remaining portion of each section was fixed in 10 % NBF for immunostaining. Each piece of tissue was weighed and the amount of ASO was then measured by various bioanalytical methods (Yu et al., 2013), including capillary gel electrophoresis coupled with UV detection (CGE-UV), high performance liquid chromatography coupled with UV detection (HPLC-UV), high performance liquid chromatography coupled with tandem mass spectrometry detection (HPLC-MS/MS) or a hybridization-based enzyme-linked immunosorbent assay (HELISA). For HELISA, the probe has the sequence complementary to ISIS 396443 containing Biotin-TEG at the 5' end and digoxigenin at the 3' end.

Immunostaining. Staining of the ASO and SMN protein in mouse tissues was performed as previously described (Hua et al., 2010). Staining of ASO in non-human primate tissues was

JPET Fast Forward. Published on April 30, 2014 as DOI: 10.1124/jpet.113.212407
This article has not been copyedited and formatted. The final version may differ from this version.

performed as previously described (Kordasiewicz et al., 2012).

Plasma chemistry. Plasma alanine aminotransferase (ALT), aspartate aminotransferase (AST), and blood urea nitrogen (BUN) concentrations were quantified on an Olympus AU400e automated clinical chemistry analyzer (Melville, NY).

Data analysis. The ED_{50} was calculated using GraphPad Prism Version 6.0 or higher (GraphPad Software, San Diego, CA) after fitting the data using non-linear regression with normalized response and variable slope. The ED_{50} was not calculated for experiments with a three-point dose response. The EC_{50} and IC_{50} (half-maximal inhibitory concentration) were determined after fitting the data points to a sigmoidal E_{max} model or sigmoidal I_{max} model, respectively, using Phoenix WinNonlin 6.0 or higher software (Pharsight Corporation, Mountain View, CA). For EC_{50} and IC_{50} determinations, E_0 values were fixed to be near 1.0 (0.8 to 1.2) to improve the curve fit. In addition, EC_{50} and IC_{50} values were bounded to be within reasonable physiological limits. The tissue half-life of ISIS 396443 associated with the apparent terminal elimination phase was calculated using a non-compartmental analysis extravascular input model applied to the mean concentration-time profile using Phoenix WinNonlin, Version 6.0 or higher (Pharsight Corporation, Mountain View, CA).

JPET Fast Forward. Published on April 30, 2014 as DOI: 10.1124/jpet.113.212407
This article has not been copyedited and formatted. The final version may differ from this version.

Results

ICV infusion versus ICV bolus injection of ISIS 396443 in rodents

Previously we demonstrated that administration of ISIS 396443 by intracerebroventricular (ICV) infusion into the cerebrospinal fluid (CSF) of adult mice transgenic for human *SMN2* results in almost complete *SMN2* exon 7 inclusion in CNS tissues (**Fig. 1A and Supplemental Fig. 1A**) (Hua et al., 2010). However, for phenotypic rescue experiments in mouse models of severe SMA, which required treating neonatal mice, we administered ISIS 396443 by ICV bolus injection (Hua et al., 2011; Passini et al., 2011). Here we directly compared the two methods of administration in adult homozygous SMA mice (*Smn*$^{-/-}$; *SMN2*$^{+/+}$) (Hsieh-Li et al., 2000) with four copies of an *SMN2* transgene to determine which method of delivery was most efficient. Increasing doses of ISIS 396443 ASO were infused into the CSF for 7 days (**Fig. 1A**) or administered as a single ICV bolus injection (**Fig. 1D**). Tissues were analyzed for *SMN2* splicing 2 days after the end of the infusion or 9 days after a single bolus injection, using real-time RT-PCR. For both methods of delivery, administration of ISIS 396443 resulted in a dose-dependent increase in *SMN2* splicing correction, observed as an increase in transcripts including exon 7 and a decrease in transcripts excluding exon 7, in both the spinal cord (**Figs. 1A, D**) and the brain (**Supplemental Figs. 1A, D**). We also examined *SMN2* splicing 71 days after the end of the 30 μg/day ICV infusion and found that the level of correction in the spinal cord and brain (data not shown) was comparable to the level observed 2 days after the end of the infusion (**Fig. 1A and Supplemental Fig. 1A**). However, the ICV bolus injection was a more efficient method of delivery, based on the half-maximal effective dose (ED_{50}). The ED_{50} for *SMN2* exon 7 inclusion following ICV bolus injection was calculated to be 17 μg for the spinal cord (**Fig. 1D**) and 35 μg for the brain (**Supplemental Fig. 1D**) compared 105 μg (15 μg/day) for the spinal cord (**Fig. 1A**)

JPET Fast Forward. Published on April 30, 2014 as DOI: 10.1124/jpet.113.212407
This article has not been copyedited and formatted. The final version may differ from this version.

and 147 μg (21 μg/day) for the brain (**Supplemental Fig. 1A**) when ISIS 396443 was administered by ICV infusion.

We also examined the relationship between the amount of ISIS 396443 in CNS tissue and the degree of *SMN2* splicing correction after both ICV infusion and ICV bolus injection. For each mouse that was dosed in **Figs. 1A, D**, we measured the amount of ISIS 396443 in CNS tissue using high performance liquid chromatography coupled with ultraviolet detection (HPLC-UV) or a hybridization-based enzyme-linked immunosorbent assay (HELISA), and this was plotted against the level of transcripts including exon 7 or the level of transcripts excluding exon 7 in the spinal cord and brain of the same mouse. For both routes of administration, we observed a good correlation between the amount of ISIS 396443 in CNS tissue and the levels *SMN2* splicing correction for the spinal cord (**Figs. 1B, E**) and brain (**Supplemental Figs. 1B, E**). However, the ICV bolus injection of ISIS 396443 was a more efficient method of delivery, based on the half-maximal effective concentration (EC_{50}). The EC_{50} was calculated to be 1.6 μg of ISIS 396443 per gram of spinal cord tissue (1.6 μg/g) (**Fig. 1E**) and 5.7 μg/g for the brain (**Supplemental Fig. 1E**) compared to 9.3 μg/g for the spinal cord (**Fig. 1B**) and 20.2 μg/g for the brain (**Supplemental Fig. 1B**) when ISIS 396443 was administered by ICV infusion. Similar EC_{50} values for the spinal cord (1.2 μg/g) and brain (3.7 μg/g) were obtained when ISIS 396443 was injected by ICV bolus to the C/C mouse model (Osborne et al., 2012) (**Supplemental Figs. 3B, E**). Interestingly, when ISIS 396443 was administered by intraperitoneal (IP) bolus injection, the EC_{50} value (135 μg/g) obtained in the liver was considerably higher (**Supplemental Fig. 4B**).

We evaluated the CNS tissue distribution of ISIS 396443 after ICV bolus injection. The localization of ISIS 396443 was determined by immunohistochemistry (IHC) 9 days after a 350 μg injection. ISIS 396443 distributed broadly throughout the spinal cord and brain, with

JPET Fast Forward. Published on April 30, 2014 as DOI: 10.1124/jpet.113.212407
This article has not been copyedited and formatted. The final version may differ from this version.

accumulation in cortical, striatal, hippocampal and motor neurons (**Supplemental Fig. 2A)**. Consistent with the accumulation of ISIS 396443 in CNS tissues (**Supplemental Fig. 2A**) and efficient correction of *SMN2* splicing (**Fig. 1D and Supplemental Fig. 1D**), we also observed elevated levels of SMN protein in the spinal cord and brain, as determined by IHC (**Supplemental Fig. 2B**).

We also determined if administration of ISIS 396443 by either ICV infusion or ICV bolus injection (Figure 1) resulted in the induction of allograft inflammatory factor-1 (*Aif1*), a marker of monocyte/microglial activation. We examined the expression of *Aif1* in CNS tissues using real-time RT–PCR. Regardless of the method of administration, we observed no marked increase of *Aif1* transcripts in the spinal cord (**Figs. 1C, F**) and brain (**Supplemental Figs. 1C, F**) (Hua et al., 2010) at any dose of ISIS 396443 tested.

ISIS 396443 duration of action after ICV infusion or ICV bolus injection in rodents

Previously we demonstrated that a 7-day ICV infusion of ISIS 396443 at 50 μg/day resulted in sustained *SMN2* splicing correction for up to 6 months (Hua et al., 2010). To determine if *SMN2* splicing correction could be maintained for a longer period of time, adult *SMN2* transgenic mice were treated by ICV infusion with 50 μg/day for 7 days (350 μg total) and *SMN2* splicing was measured by real-time RT-PCR in the spinal cord and brain at various time points. Following ICV infusion of ISIS 396443, *SMN2* splicing correction in the spinal cord (**Fig. 2A**) and brain (**Supplemental Fig. 5A**) were maintained for at least 1 year, with no signs of microglial activation (**Fig. 2B and Supplemental Fig. 5B**). A single ICV bolus injection of 100 μg of ISIS 396443 also resulted in prolonged pharmacological activity that was maintained for at least 36 weeks post-dosing, in the spinal cord (**Fig. 2D**) and brain (**Supplemental Fig. 5C**)

JPET Fast Forward. Published on April 30, 2014 as DOI: 10.1124/jpet.113.212407
This article has not been copyedited and formatted. The final version may differ from this version.

without causing microglial activation (**Fig. 2E and Supplemental Fig. 5D**). Similar results were obtained with an ICV bolus injection of 25 μg (**Supplemental Figs. 6A-D**). In contrast, the duration of action of ISIS 396443 in the liver after IP bolus injection was much shorter, with minimal *SMN2* splicing correction observed 8 weeks after dosing (**Supplemental Fig. 9A**).

Since the pharmacological effects of ISIS 396443 lasted many months, we wondered if the levels of ISIS 396443 in CNS tissues changed over time. We measured the ASO levels in the spinal cord and brain by HPLC-UV or HELISA at various time points after the ICV infusion or ICV bolus injection and calculated the tissue half-life. Both the ICV infusion and ICV bolus injection of ISIS 396443 yielded a tissue half-life of over 100 days in the spinal cord and the brain (**Fig. 2C, F and Supplemental Fig. 6E**). Therefore, the long-lasting pharmacodynamic effects of ISIS 396443 can be attributed to its long tissue half-life. For many months after dosing, ISIS 396443 remains at sufficient levels in CNS tissues to modulate splicing. Mass spectrometry analysis of CNS tissues indicated minimal metabolism of ISIS 396443, with the main metabolite being the parent compound that lacked a 3'-terminal guanosine (data not shown). In agreement with the long pharmacological effects and tissue half-life, ISIS 396443 could be detected in motor neurons 1 year after the 7-day ICV infusion and 36 weeks after the ICV bolus injection (**Supplemental Figs. 7A and 8A**). In addition, SMN protein was also present in motor neurons at these time points (**Supplemental Figs. 7B and 8B**). In contrast to what was observed in the CNS, the liver half-life of ISIS 396443 was about 20 days (**Supplemental Fig. 9B**), in agreement with the shorter duration of *SMN2* splicing correction in liver.

The long-lasting pharmacodynamic effects of ISIS 396443 in the CNS of mice are in agreement with its long tissue half-life. However, to confirm that the *SMN2* splicing correction was still driven by the presence of ISIS 396443 after its delivery, we administered a fully

JPET Fast Forward. Published on April 30, 2014 as DOI: 10.1124/jpet.113.212407
This article has not been copyedited and formatted. The final version may differ from this version.

complementary oligonucleotide decoy (α443) to neutralize its effects. Three weeks after a 100 μg ICV bolus injection of ISIS 396443, efficient *SMN2* splicing correction was observed in the spinal cord and brain (**Supplemental Figs. 10A, C**). At this time point we administered 400 μg of the complementary oligonucleotide decoy, α443, by ICV bolus injection and assessed the effects on *SMN2* splicing two weeks later. Administration of α443 reversed the ISIS 396443-mediated splicing correction in the spinal cord and brain (**Supplemental Figs. 10A, C)**. Similar results were obtained when lower doses of ISIS 396443 and α443 were used (**Supplemental Figs. 10B, D**).

ISIS 396443 versus 2'-OMe, morpholino and cEt ASOs in the CNS of rodents

ASOs with 2'-*O*-methoxyethyl (2'-MOE) (Hua et al., 2011; Passini et al., 2011), 2'-*O*-methyl (2'-OMe) (Williams et al., 2009) and phosphorodiamindate morpholino (PMO) chemistries (Porensky et al., 2011; Mitrpant et al., 2013; Zhou et al., 2013) (**Fig. 3A**), that drive *SMN2* exon 7 inclusion, have been tested in mice with severe SMA by central administration within the first postnatal day. In these experiments early administration of the ASOs was necessary since severe SMA mice normally die within the first weeks of life. To more adequately compare the potency of ASOs with different chemistries, in order to select the best ASO to advance into clinical trials, we administered them centrally to adult mice. We tested ISIS 396443, an 18-mer ASO with the 2'-MOE chemistry (Hua et al., 2008; Hua et al., 2010; Hua et al., 2011; Passini et al., 2011), and two 20-mer ASOs of the same sequence: a 2'-OMe ASO (Singh et al., 2006; Williams et al., 2009), and a PMO ASO (Porensky et al., 2011; Mitrpant et al., 2013) that were previously optimized for *SMN2* exon 7 inclusion and like ISIS 396443 also target ISS-N1. Increasing doses of these ASOs were administred by a single ICV bolus injection to adult *SMN2* transgenic mice

JPET Fast Forward. Published on April 30, 2014 as DOI: 10.1124/jpet.113.212407
This article has not been copyedited and formatted. The final version may differ from this version.

and *SMN2* splicing correction was measured by real-time RT-PCR 9 days later in CNS tissues. Consistent with our previous report (Hua et al., 2010), administration of the 2'-OMe ASO did not result in *SMN2* splicing correction in the spinal cord (**Fig. 3B**) and brain (**Supplemental Fig. 12A**) but did elevate *Aif1* expression in the spinal cord (**Supplemental Fig. 12D**). In this experiment, the 2'-OMe ASO did accumulate in spinal cord and brain tissue, in a dose-dependent manner, to a similar level as ISIS 396443 (**Fig. 3C and Supplemental Fig. 12B**). In addition, this 2'-OMe ASO was able to correct *SMN2* splicing when administered to SMA fibroblasts by lipid transfection (**Supplemental Fig. 11A**), but surprisingly, it was almost completely inactive when administered by electroporation (**Supplemental Fig. 11C**).

Administration of the PMO-20 ASO resulted in a dose-dependent increase in *SMN2* splicing correction in the spinal cord (**Fig. 3D**) and brain (**Supplemental Fig. 14A**). However, the PMO-20 ASO was not as potent as ISIS 396443 when administered to adult *SMN2* transgenic mice. For the PMO-20 ASO, the ED_{50} for *SMN2* exon 7 inclusion was calculated to be 102 μg for the spinal cord and 65 μg for the brain. This represents a 3-5 fold decrease in potency, as the ED_{50} for ISIS 396443 in the same experiment was calculated to be 19 μg for the spinal cord and 18 μg for the brain (**Fig. 3D and Supplemental Fig. 14A**). The same conclusion was reached when we tested another PMO ASO that was slightly longer (PMO-23) (**Supplemental Fig. 15**). In contrast, when the ASOs were administered to SMA patient fibroblasts the PMO-20 ASO was as potent as ISIS 396443 for *SMN2* splicing correction (**Supplemental Fig. 11B**).

To determine if the reduced potency of the PMO-20 ASO for *SMN2* splicing correction in transgenic mice was due to its accumulation in the CNS, we measured its levels in the spinal cord and brain by HELISA. The accumulation of the PMO-20 ASO in CNS tissues was substantially lower, compared to ISIS 396443 in the spinal cord (**Fig. 3E**) and brain

JPET Fast Forward. Published on April 30, 2014 as DOI: 10.1124/jpet.113.212407
This article has not been copyedited and formatted. The final version may differ from this version.

(**Supplemental Fig. 14B**). When we plotted the concentration of the PMO-20 ASO in the spinal cord and brain as a function of the level of *SMN2* splicing correction, we found that its EC_{50} was lower compared to ISIS 396443: 0.3 μg/g vs. 1.4 μg/g in the spinal cord (**Fig. 3F and Supplemental Fig. 13**) and 0.8 μg/g vs. 6.3 μg/g in the brain (**Supplemental Fig. 14C, D**). These findings suggest that the PMO-20 ASO has less efficient tissue retention or cellular uptake than ISIS 396443. However the smaller amount of PMO-20 ASO that is retained in tissue or taken up by cells can efficiently correct *SMN2* splicing.

The binding affinity of an ASO to its target can be increased dramatically by the incorporation of 2',4'-bridged nucleic acid modifications such as locked nucleic acid (LNA) (Vester and Wengel, 2004) and 2',4'-constrained 2'-O-ethyl (cEt) (Seth et al., 2010) (**Fig. 3A**). We determined if a cEt-modified version of ISIS 396443 was more active than ISIS 396443. We tested a cEt mixmer (2'-MOE/cEt) ASO with a melting temperature 15^{o}C higher than ISIS 396443 in SMA fibroblasts and found that its potency was similar to ISIS 396443 (**Supplemental Fig. 11C**). This was also the case when we administered the 2'-MOE/cEt ASO by ICV bolus injection to adult *SMN2* transgenic mice (**Fig. 3G and Supplemental Fig. 16**). Therefore, further increasing the affinity of ISIS 396443 for binding to ISS-N1 does not increase its potency for *SMN2* splicing correction

Pharmacokinetics of ISIS 396443 in the CNS of non-human primates

NHPs do not have the *SMN2* gene (Rochette et al., 2001) and rely on the *SMN1* gene for SMN protein production. In humans, about 10 % of the transcripts produced from the *SMN1* gene exclude exon 7 (Lorson et al., 1999). We reasoned that if exon 7 skipped transcripts from the NHP *SMN1* gene could be detected in the spinal cord, we could potentially evaluate ASO-

JPET Fast Forward. Published on April 30, 2014 as DOI: 10.1124/jpet.113.212407
This article has not been copyedited and formatted. The final version may differ from this version.

mediated *SMN1* splicing correction in a large animal. Unfortunately, we could not detect *SMN1* exon 7 skipped transcripts in the spinal cord (**Supplemental Fig. 17**), precluding our ability to measure pharmacodynamic effects of ISIS 396443 in NHPs. Instead, we determined if administration of ISIS 396443 to NHPs by intrathecal (IT) bolus injection resulted in a spinal cord ASO concentration that was predicted to achieve the EC_{50} (~1 μg/g) for *SMN2* splicing correction in the spinal cord of *SMN2* transgenic mice after delivery of ISIS 396443 by ICV bolus. IT bolus injection is technically challenging in mice but is feasible in non-human primates. Adult cynomolgus monkeys were treated by a single IT bolus injection with either 1, 3 or 7 mg of ISIS 396443 and tissues were collected 7 days after dosing for processing. The accumulation of ISIS 396443 in CNS tissues was dose-dependent, with greater accumulation in the spinal cord and cortex (**Fig. 4A**). Even at the 1 mg dose, the levels of ISIS 396443 in the spinal cord exceeded the targeted tissue concentration of about 1 μg/g by 3 to 8 fold. Immunohistochemical staining of various regions of the spinal cord and brain for the presence of ISIS 396443 showed broad distribution of ISIS 396443, with the greatest accumulation in large and small cell bodies of the grey matter, consistent with neuronal and glial cell targeting (**Figs. 4B-D**). Hematoxylin and eosin (H&E) staining did not reveal any pathological findings at the doses of ISIS 396443 tested (data not shown).

JPET Fast Forward. Published on April 30, 2014 as DOI: 10.1124/jpet.113.212407
This article has not been copyedited and formatted. The final version may differ from this version.

Discussion

Here we determined that, on a per-dose basis, ISIS 396443 is the most potent ASO for *SMN2* splicing correction in the CNS of adult mice out of several ASOs tested, including an ASO with high-binding affinity chemical modifications. The most efficient method of delivering ISIS 396443 to the CNS of rodents is through an ICV bolus injection, with pharmacology in CNS tissues that is long-lasting. In addition, administration of ISIS 396443 to the CNS of NHPs by a single IT bolus injection results in widespread distribution throughout the spinal cord and accumulation to levels predicted to be pharmacologically active, based upon our experiments in rodents. Based upon our complete set of preclinical studies, we have advanced ISIS 396443 into clinical development.

There are several reasons why IT bolus injection of ISIS 396443, rather than an infusion, is being pursued in the clinic, based in part on the present study: 1) bolus injection results in potent and efficient *SMN2* splicing correction in the CNS of rodents; 2) bolus injection results in sustained *SMN2* splicing correction in the CNS of rodents for many months, which can be extrapolated to infrequent dosing in the clinic; 3) bolus injection results in distribution of the ASO throughout the spinal cord of NHPs and accumulation in tissue at levels predicted to be pharmacologically active. In addition, for IT delivery of ISIS 396443 to SMA patients, the implantation of an infusion device (i.e. an implanted pump) is not feasible in small children or infants, whereas standard lumbar puncture (LP) bolus injections have been proven to be feasible and well tolerated in children (i.e. for the delivery of anesthetics and chemotherapeutics). In fact, an administration of a single dose of ISIS 396443 by LP bolus injection in children with SMA aged 2 to 14 years of age has recently been shown to be feasible and well tolerated in a completed Phase 1 clinical study (Chirboga et al., 2013).

Previous studies indicate that ASOs accumulate in cells and tissues by at least two distinct uptake pathways (Bennett and Swayze, 2010). One pathway is termed the productive uptake pathway, which ultimately results in the productive engagement of the ASO with the desired target. The second pathway is a nonproductive pathway that acts as a saturable sink and impairs the ability of the ASO to reach the productive pathway. It is likely that many different non-productive sinks exist, but some have been described as intracellular lysosomes, cell-surface proteins or even other cell types (Geary et al., 2009; Koller et al., 2011; Ming et al., 2013). Several of our results may be explained by preferential utilization of the productive versus nonproductive ASO uptake pathway. The EC_{50} for *SMN2* splicing correction is an indicator of the amount of drug taken up into tissues via productive uptake. The lower EC_{50} in CNS tissues compared to liver when ISIS 396443 was administered centrally versus peripherally, respectively, suggests that ISIS 396443 favors a productive uptake pathway in the CNS, compared to liver. The lower EC_{50} in CNS tissues when ISIS 396443 was administered by ICV bolus injection, which results in a higher maximum concentration in CSF, versus ICV infusion, suggests that delivery of ISIS 396443 by ICV bolus injection results in greater productive uptake. Perhaps the scenario in the CNS is similar to what has been observed for the liver, where administration by slow infusion results in the preferential accumulation of ASO in a nonproductive compartment (Geary et al., 2009). The lower EC_{50} for the PMO ASO versus ISIS 396443 in CNS tissues implies that a greater fraction of the PMO ASO in the tissue is found in a productive compartment, despite its diminished overall tissue accumulation, compared to ISIS 396443. Taken together, our results demonstrate that the preferential utilization of the productive uptake pathway depends on the target tissue, the method of delivery and the chemistry of the ASO.

The prolonged duration of *SMN2* splicing correction after a single ICV bolus injection is in agreement with the slow clearance of ISIS 396443 from CNS tissues, which remains at sufficient levels to maximally correct *SMN2* splicing for many months. Because ISIS 396443 is fully modified with 2'-MOE nucleotides that confer increased nuclease resistance (Teplova et al., 1999), we expected the long tissue half-lives. However, low ASO metabolic activity in CNS tissues might also be a contributing factor (Whitesell et al., 1993). It is also interesting to consider that the long duration of antisense effects in the CNS might be attributable to the target cells being post-mitotic, as long-lasting pharmacology has also been observed in muscle (Wheeler et al., 2012).

In light of the finding that ISIS 396443 is more potent for *SMN2* splicing correction in CNS tissues of adult transgenic mice compared to PMO ASOs, the longer survival conferred by ICV-injected PMO ASOs (Porensky et al., 2011; Mitrpant et al., 2013; Zhou et al., 2013) compared to ISIS 396443 (Hua et al., 2011; Passini et al., 2011) in severe SMA mice is intriguing. Several possibilities may account for this paradox, including the higher doses of PMO ASOs used in neonatal mice, the longer duration of PMO ASO-mediated *SMN2* splicing correction in a growing neonatal mouse, the higher exposure of peripheral tissues to PMO ASOs after CNS administration, or enhanced activity of the PMO ASOs in certain CNS cell types. Additional studies are necessary to address the apparent paradox.

JPET Fast Forward. Published on April 30, 2014 as DOI: 10.1124/jpet.113.212407
This article has not been copyedited and formatted. The final version may differ from this version.

Acknowledgments

We thank the ISIS ASO synthesis group and Thazha Prakash for ASO synthesis, and the SMA Foundation for providing the C/C mice.

Authorship Contributions

Participated in research design: Rigo, Chun, Fey, Hua, Grundy, Krainer, Henry, Bennett.

Conducted experiments: Rigo, Chun, Lee.

Contributed new reagents or analytical tools:

Performed data analysis: Rigo, Chun, Norris, Hung, Matson, Gaus.

Wrote or contributed to the writing of the manuscript: Rigo, Krainer, Bennett

References

Bebee TW, Dominguez CE and Chandler DS (2012) Mouse models of SMA: tools for disease characterization and therapeutic development. *Human genetics.*

Bennett CF and Swayze EE (2010) RNA targeting therapeutics: molecular mechanisms of antisense oligonucleotides as a therapeutic platform. *Annu Rev Pharmacol Toxicol* **50**:259-293.

Burghes AH and Beattie CE (2009) Spinal muscular atrophy: why do low levels of survival motor neuron protein make motor neurons sick? *Nat Rev Neurosci* **10**:597-609.

Cartegni L and Krainer AR (2003) Correction of disease-associated exon skipping by synthetic exon-specific activators. *Nat Struct Biol* **10**:120-125.

Chirboga C, Swoboda K, Darras B, Iannaccone S, Montes J, Allen H, Parad R, Johnson S, De Vivo D, Norris D, Alexander K, Bennett F and Bishop K (2013) Results of an open-label, escalating dose study to assess the safety, tolerability, and dose range finding of a single intrathecal dose of ISIS-SMNRx in patients with spinal muscular atrophy, in *65th American Academy of Neurology Annual Meeting, abstract S36002*.

Cho S and Dreyfuss G (2010) A degron created by SMN2 exon 7 skipping is a principal contributor to spinal muscular atrophy severity. *Genes Dev* **24**:438-442.

Coady TH and Lorson CL (2010) Trans-splicing-mediated improvement in a severe mouse model of spinal muscular atrophy. *J Neurosci* **30**:126-130.

Coady TH, Shababi M, Tullis GE and Lorson CL (2007) Restoration of SMN function: delivery of a trans-splicing RNA re-directs SMN2 pre-mRNA splicing. *Molecular therapy : the journal of the American Society of Gene Therapy* **15**:1471-1478.

Coovert DD, Le TT, McAndrew PE, Strasswimmer J, Crawford TO, Mendell JR, Coulson SE, Androphy EJ, Prior TW and Burghes AH (1997) The survival motor neuron protein in spinal muscular atrophy. *Human molecular genetics* **6**:1205-1214.

Crawford TO and Pardo CA (1996) The neurobiology of childhood spinal muscular atrophy. *Neurobiology of disease* **3**:97-110.

Dickson A, Osman E and Lorson CL (2008) A negatively acting bifunctional RNA increases survival motor neuron both in vitro and in vivo. *Human gene therapy* **19**:1307-1315.

Feldkotter M, Schwarzer V, Wirth R, Wienker TF and Wirth B (2002) Quantitative analyses of SMN1 and SMN2 based on real-time lightCycler PCR: fast and highly reliable carrier testing and prediction of severity of spinal muscular atrophy. *Am J Hum Genet* **70**:358-368.

Foust KD, Wang X, McGovern VL, Braun L, Bevan AK, Haidet AM, Le TT, Morales PR, Rich MM, Burghes AH and Kaspar BK (2010) Rescue of the spinal muscular atrophy phenotype in a mouse model by early postnatal delivery of SMN. *Nat Biotechnol* **28**:271-274.

Geary RS, Wancewicz E, Matson J, Pearce M, Siwkowski A, Swayze E and Bennett F (2009) Effect of dose and plasma concentration on liver uptake and pharmacologic activity of a 2'-methoxyethyl modified chimeric antisense oligonucleotide targeting PTEN. *Biochemical pharmacology* **78**:284-291.

Geib T and Hertel KJ (2009) Restoration of full-length SMN promoted by adenoviral vectors expressing RNA antisense oligonucleotides embedded in U7 snRNAs. *PLoS One* **4**:e8204.

Hamilton G and Gillingwater TH (2013) Spinal muscular atrophy: going beyond the motor neuron. *Trends in molecular medicine* **19**:40-50.

Hsieh-Li HM, Chang JG, Jong YJ, Wu MH, Wang NM, Tsai CH and Li H (2000) A mouse model for spinal muscular atrophy. *Nat Genet* **24**:66-70.

Hua Y and Krainer AR (2012) Antisense-mediated exon inclusion. *Methods Mol Biol* **867**:307-323.

Hua Y, Sahashi K, Hung G, Rigo F, Passini MA, Bennett CF and Krainer AR (2010) Antisense correction of SMN2 splicing in the CNS rescues necrosis in a type III SMA mouse model. *Genes Dev* **24**:1634-1644.

Hua Y, Sahashi K, Rigo F, Hung G, Horev G, Bennett CF and Krainer AR (2011) Peripheral SMN restoration is essential for long-term rescue of a severe spinal muscular atrophy mouse model. *Nature* **478**:123-126.

Hua Y, Vickers TA, Baker BF, Bennett CF and Krainer AR (2007) Enhancement of SMN2 exon 7 inclusion by antisense oligonucleotides targeting the exon. *PLoS Biol* **5**:e73.

Hua Y, Vickers TA, Okunola HL, Bennett CF and Krainer AR (2008) Antisense masking of an hnRNP A1/A2 intronic splicing silencer corrects SMN2 splicing in transgenic mice. *Am J Hum Genet* **82**:834-848.

Koller E, Vincent TM, Chappell A, De S, Manoharan M and Bennett CF (2011) Mechanisms of single-stranded phosphorothioate modified antisense oligonucleotide accumulation in hepatocytes. *Nucleic Acids Res* **39**:4795-4807.

Kordasiewicz HB, Stanek LM, Wancewicz EV, Mazur C, McAlonis MM, Pytel KA, Artates JW, Weiss A, Cheng SH, Shihabuddin LS, Hung G, Bennett CF and Cleveland DW (2012) Sustained Therapeutic Reversal of Huntington's Disease by Transient Repression of Huntingtin Synthesis. *Neuron* **74**:1031-1044.

Lefebvre S, Burglen L, Reboullet S, Clermont O, Burlet P, Viollet L, Benichou B, Cruaud C, Millasseau P, Zeviani M and et al. (1995) Identification and characterization of a spinal muscular atrophy-determining gene. *Cell* **80**:155-165.

Lefebvre S, Burlet P, Liu Q, Bertrandy S, Clermont O, Munnich A, Dreyfuss G and Melki J (1997) Correlation between severity and SMN protein level in spinal muscular atrophy. *Nat Genet* **16**:265-269.

Lim SR and Hertel KJ (2001) Modulation of survival motor neuron pre-mRNA splicing by inhibition of alternative 3' splice site pairing. *J Biol Chem* **276**:45476-45483.

Lorson CL, Hahnen E, Androphy EJ and Wirth B (1999) A single nucleotide in the SMN gene regulates splicing and is responsible for spinal muscular atrophy. *Proc Natl Acad Sci U S A* **96**:6307-6311.

Lunn MR and Wang CH (2008) Spinal muscular atrophy. *Lancet* **371**:2120-2133.

Meyer K, Marquis J, Trub J, Nlend Nlend R, Verp S, Ruepp MD, Imboden H, Barde I, Trono D and Schumperli D (2009) Rescue of a severe mouse model for spinal muscular atrophy by U7 snRNA-mediated splicing modulation. *Human molecular genetics* **18**:546-555.

Ming X, Carver K, Fisher M, Noel R, Cintrat JC, Gillet D, Barbier J, Cao C, Bauman J and Juliano RL (2013) The small molecule Retro-1 enhances the pharmacological actions of antisense and splice switching oligonucleotides. *Nucleic Acids Res* **41**:3673-3687.

Mitrpant C, Porensky P, Zhou H, Price L, Muntoni F, Fletcher S, Wilton SD and Burghes AH (2013) Improved antisense oligonucleotide design to suppress aberrant SMN2 gene transcript processing: towards a treatment for spinal muscular atrophy. *PLoS One* **8**:e62114.

Miyajima H, Miyaso H, Okumura M, Kurisu J and Imaizumi K (2002) Identification of a cis-acting element for the regulation of SMN exon 7 splicing. *J Biol Chem* **277**:23271-23277.

Monani UR, Lorson CL, Parsons DW, Prior TW, Androphy EJ, Burghes AH and McPherson JD (1999) A single nucleotide difference that alters splicing patterns distinguishes the SMA gene SMN1 from the copy gene SMN2. *Human molecular genetics* **8**:1177-1183.

Monani UR, Sendtner M, Coovert DD, Parsons DW, Andreassi C, Le TT, Jablonka S, Schrank B, Rossoll W, Prior TW, Morris GE and Burghes AH (2000) The human centromeric survival motor neuron gene (SMN2) rescues embryonic lethality in Smn(-/-) mice and results in a mouse with spinal muscular atrophy. *Human molecular genetics* **9**:333-339.

Osborne M, Gomez D, Feng Z, McEwen C, Beltran J, Cirillo K, El-Khodor B, Lin MY, Li Y, Knowlton WM, McKemy DD, Bogdanik L, Butts-Dehm K, Martens K, Davis C, Doty R, Wardwell K, Ghavami A, Kobayashi D, Ko CP, Ramboz S and Lutz C (2012) Characterization of behavioral and neuromuscular junction phenotypes in a novel allelic series of SMA mouse models. *Human molecular genetics*.

Osman EY, Yen PF and Lorson CL (2012) Bifunctional RNAs Targeting the Intronic Splicing Silencer N1 Increase SMN Levels and Reduce Disease Severity in an Animal Model of Spinal Muscular Atrophy. *Molecular therapy : the journal of the American Society of Gene Therapy* **20**:119-126.

Passini MA, Bu J, Richards AM, Kinnecom C, Sardi SP, Stanek LM, Hua Y, Rigo F, Matson J, Hung G, Kaye EM, Shihabuddin LS, Krainer AR, Bennett CF and Cheng SH (2011) Antisense oligonucleotides delivered to the mouse CNS ameliorate symptoms of severe spinal muscular atrophy. *Sci Transl Med* **3**:72ra18.

Passini MA, Bu J, Roskelley EM, Richards AM, Sardi SP, O'Riordan CR, Klinger KW, Shihabuddin LS and Cheng SH (2010) CNS-targeted gene therapy improves survival and motor function in a mouse model of spinal muscular atrophy. *J Clin Invest* **120**:1253-1264.

Porensky PN, Mitrpant C, McGovern VL, Bevan AK, Foust KD, Kaspar BK, Wilton SD and Burghes AH (2011) A single administration of morpholino antisense oligomer rescues spinal muscular atrophy in mouse. *Human molecular genetics*.

Prior TW, Swoboda KJ, Scott HD and Hejmanowski AQ (2004) Homozygous SMN1 deletions in unaffected family members and modification of the phenotype by SMN2. *American journal of medical genetics Part A* **130A**:307-310.

Rigo F, Hua Y, Chun SJ, Prakash TP, Krainer AR and Bennett CF (2012) Synthetic oligonucleotides recruit ILF2/3 to RNA transcripts to modulate splicing. *Nature chemical biology* **8**:555-561.

Rochette CF, Gilbert N and Simard LR (2001) SMN gene duplication and the emergence of the SMN2 gene occurred in distinct hominids: SMN2 is unique to Homo sapiens. *Human genetics* **108**:255-266.

Seth PP, Vasquez G, Allerson CA, Berdeja A, Gaus H, Kinberger GA, Prakash TP, Migawa MT, Bhat B and Swayze EE (2010) Synthesis and biophysical evaluation of 2',4'-constrained 2'O-methoxyethyl and 2',4'-constrained 2'O-ethyl nucleic acid analogues. *The Journal of organic chemistry* **75**:1569-1581.

Singh NK, Singh NN, Androphy EJ and Singh RN (2006) Splicing of a critical exon of human Survival Motor Neuron is regulated by a unique silencer element located in the last intron. *Mol Cell Biol* **26**:1333-1346.

Skordis LA, Dunckley MG, Yue B, Eperon IC and Muntoni F (2003) Bifunctional antisense oligonucleotides provide a trans-acting splicing enhancer that stimulates SMN2 gene expression in patient fibroblasts. *Proc Natl Acad Sci U S A* **100**:4114-4119.

Swayze EE, Siwkowski AM, Wancewicz EV, Migawa MT, Wyrzykiewicz TK, Hung G, Monia BP and Bennett CF (2007) Antisense oligonucleotides containing locked nucleic acid improve potency but cause significant hepatotoxicity in animals. *Nucleic Acids Res* **35**:687-700.

Teplova M, Minasov G, Tereshko V, Inamati GB, Cook PD, Manoharan M and Egli M (1999) Crystal structure and improved antisense properties of 2'-O-(2-methoxyethyl)-RNA. *Nat Struct Biol* **6**:535-539.

Vester B and Wengel J (2004) LNA (locked nucleic acid): high-affinity targeting of complementary RNA and DNA. *Biochemistry* **43**:13233-13241.

Wheeler TM, Leger AJ, Pandey SK, MacLeod AR, Nakamori M, Cheng SH, Wentworth BM, Bennett CF and Thornton CA (2012) Targeting nuclear RNA for in vivo correction of myotonic dystrophy. *Nature* **488**:111-115.

Whitesell L, Geselowitz D, Chavany C, Fahmy B, Walbridge S, Alger JR and Neckers LM (1993) Stability, clearance, and disposition of intraventricularly administered

oligodeoxynucleotides: implications for therapeutic application within the central nervous system. *Proc Natl Acad Sci U S A* **90**:4665-4669.

Williams JH, Schray RC, Patterson CA, Ayitey SO, Tallent MK and Lutz GJ (2009) Oligonucleotide-mediated survival of motor neuron protein expression in CNS improves phenotype in a mouse model of spinal muscular atrophy. *J Neurosci* **29**:7633-7638.

Yu RZ, Grundy JS and Geary RS (2013) Clinical pharmacokinetics of second generation antisense oligonucleotides. *Expert opinion on drug metabolism & toxicology* **9**:169-182.

Zhou H, Janghra N, Mitrpant C, Dickinson RL, Anthony K, Price L, Eperon IC, Wilton SD, Morgan J and Muntoni F (2013) A Novel Morpholino Oligomer Targeting ISS-N1 Improves Rescue of Severe Spinal Muscular Atrophy Transgenic Mice. *Human gene therapy* **24**:331-342.

Footnotes

F.R., S.J.C., D.A.N., G.H., S.L., J.M., R.A.F., H.G., J.S.G., S.P.H. and C.F.B. are employees of ISIS Pharmaceuticals. A.R.K. serves on the scientific advisory board of two nonprofit SMA foundations, and is a consultant for ISIS Pharmaceuticals.

JPET Fast Forward. Published on April 30, 2014 as DOI: 10.1124/jpet.113.212407
This article has not been copyedited and formatted. The final version may differ from this version.

Figure Legends

Figure 1 Administration of ISIS 396443 by ICV infusion or ICV bolus injection. (**A**) Real-time RT-PCR analysis of *SMN2* transcripts including exon 7 (FL) or excluding exon 7 (Δ7) in the lumbar spinal cord, 2 days after administration of ISIS 396443 by ICV infusion for 7 days at the indicated daily doses. For each dose level, n = 5. Error bars represent the s.d. The calculated ED_{50} is shown. (**B**) For each mouse dosed in **A**, the amount of ISIS 396443 in the thoracic spinal cord was measured by HPLC-UV and this was plotted against the level of FL or Δ7 *SMN2* transcripts measured in the lumbar spinal cord of the same mouse (open circles and triangles, respectively). The calculated EC_{50} and IC_{50} values are shown. (**C**) Same as in **A**, except that the real-time RT-PCR analysis was for *Aif1* transcripts. (**D**) Real-time RT-PCR analysis of FL and Δ7 *SMN2* transcripts in the lumbar spinal cord, 9 days after administration of ISIS 396443 by a single ICV bolus injection at the indicated dose. For each dose level n = 4. Error bars represent the s.d. The calculated ED_{50} is shown. (**E**) Same as in **B**, except that the amount of ISIS 396443 in the thoracic spinal cord was measured by HELISA. (**F**) Same as in **D**, except that the real-time RT-PCR analysis was for *Aif1* transcripts. Panels **A** and **C** are reproduced with permission from Hua et al., (Hua et al., 2010) (Copyright 2010, Cold Spring Harbor Laboratory Press).

Figure 2 Duration of action after ICV infusion or ICV bolus injection of ISIS 396443. (**A**) Real-time RT-PCR analysis of *SMN2* FL and Δ7 transcripts in the lumbar spinal cord at the indicated time points after administration of ISIS 396443 by ICV infusion at 50 μg/day for 7 days. PBS, n = 4; 1 and 3 weeks, n = 5; 12 weeks, n = 6; 24 weeks n = 7; 36 weeks, n = 6; 52 weeks n = 7. Error bars represent the s.d. (**B**) Same as in **A**, except that the real-time RT-PCR analysis was for *Aif1* transcripts. (**C**) The amount of ISIS 396443 in the thoracic spinal cord or brain of each

JPET Fast Forward. Published on April 30, 2014 as DOI: 10.1124/jpet.113.212407
This article has not been copyedited and formatted. The final version may differ from this version.

mouse was measured at each time point by HPLC-UV. 1 and 3 weeks, n = 5; 12 weeks, n = 6; 24 weeks n = 7; 36 weeks, n = 6; 52 weeks n = 7. Error bars represent the s.d. The calculated tissue half-life of ISIS 396443 is shown. (**D**) Real-time RT-PCR analysis of FL and Δ7 *SMN2* transcripts in the lumbar spinal cord at the indicated time points after administration of 100 μg of ISIS 396443 by a single ICV bolus injection. For each time point, n = 5, except for the 24 weeks group, for which n = 4. Error bars represent the s.d. (**E**) Same as in **D**, except that the real-time RT-PCR analysis was for *Aif1* transcripts. (**F**) Same as in **C**, except that the amount of ISIS 396443 in the thoracic spinal cord and brain was measured by HELISA. For each time point, n = 5, except for the 24 weeks group, for which n = 4. Error bars represent the s.d.

Figure 3 Comparison of ISIS 396443 to 2'-MOE, PMO-20 and cEt ASOs. (**A**) Structures of chemically modified nucleotides. (**B**) Real-time RT-PCR analysis of FL and Δ7 *SMN2* transcripts in the lumbar spinal cord, 9 days after administration of ISIS 396443 or the 2'-OMe ASO by a single ICV bolus injection at the indicated dose. For each dose level, n = 4. Error bars represent the s.d. (**C**) The amount of ISIS 396443 and 2'-OMe ASO in the thoracic spinal cord of each mouse was measured by HELISA. For each dose level, n = 4. Error bars represent the s.d. (**D**) Same as **B**, except that ISIS 396443 and the PMO-20 ASO were administered at the indicated doses. The calculated ED_{50} is shown. (**E**) Same as in **C**, except that ISIS 396443 and the PMO-20 ASO were measured. (**F**) The concentration of the PMO-20 ASO in the thoracic spinal cord of each mouse in **E** was plotted against the level of FL or Δ7 *SMN2* transcripts measured in the lumbar spinal cord of the same mouse (open circles and triangles, respectively). The calculated EC_{50} and IC_{50} values are shown. (**G**) Same as in **B**, except that ISIS 396443 and the cEt/MOE ASO were administered at the indicated doses.

Figure 4 Pharmacokinetics of ISIS 396443 in the CNS of non-human primates after a single IT bolus injection. (**A**) The amount of ISIS 396443 in various spinal cord and brain regions of each NHP was measured by HELISA. For each dose level, n = 6. Error bars represent the s.d. (**B**-**D**) ISIS 396443 in the CNS of a primate that received a dose of 7 mg was visualized by ASO immunostaining (anti-pan ASO). Nuclei were counterstained with hematoxylin.

Figure 1

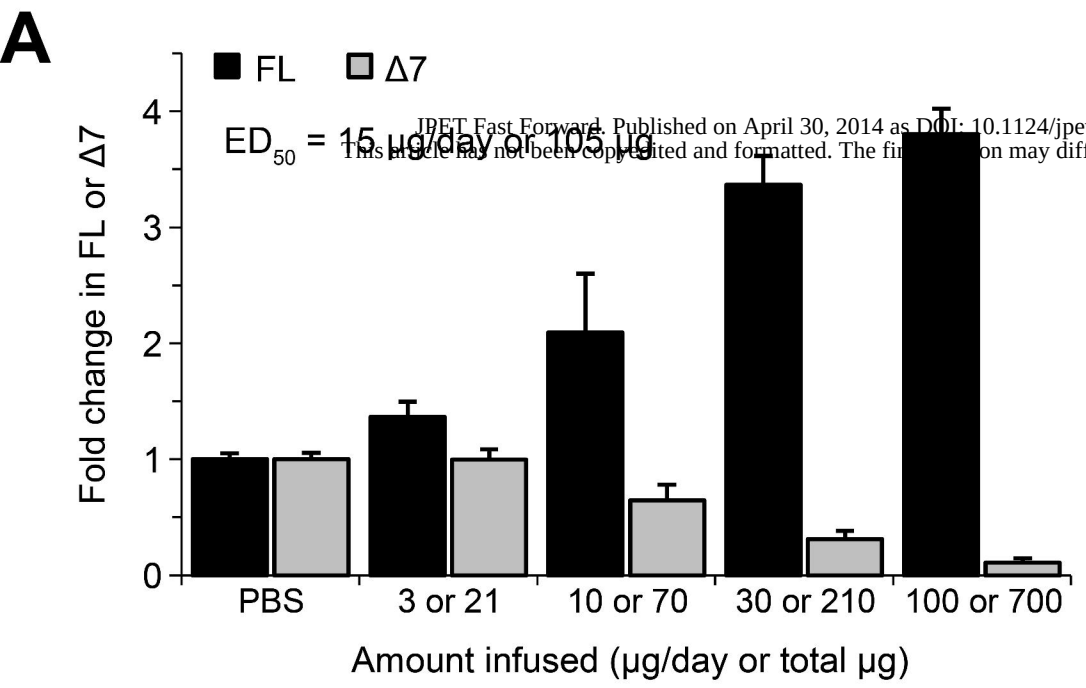

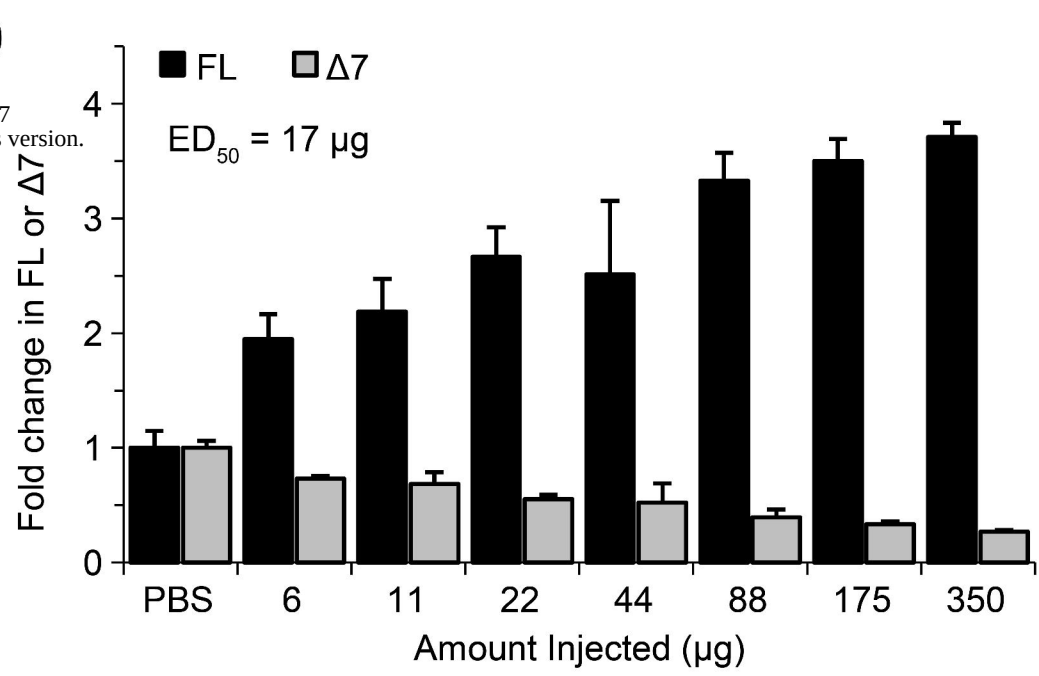

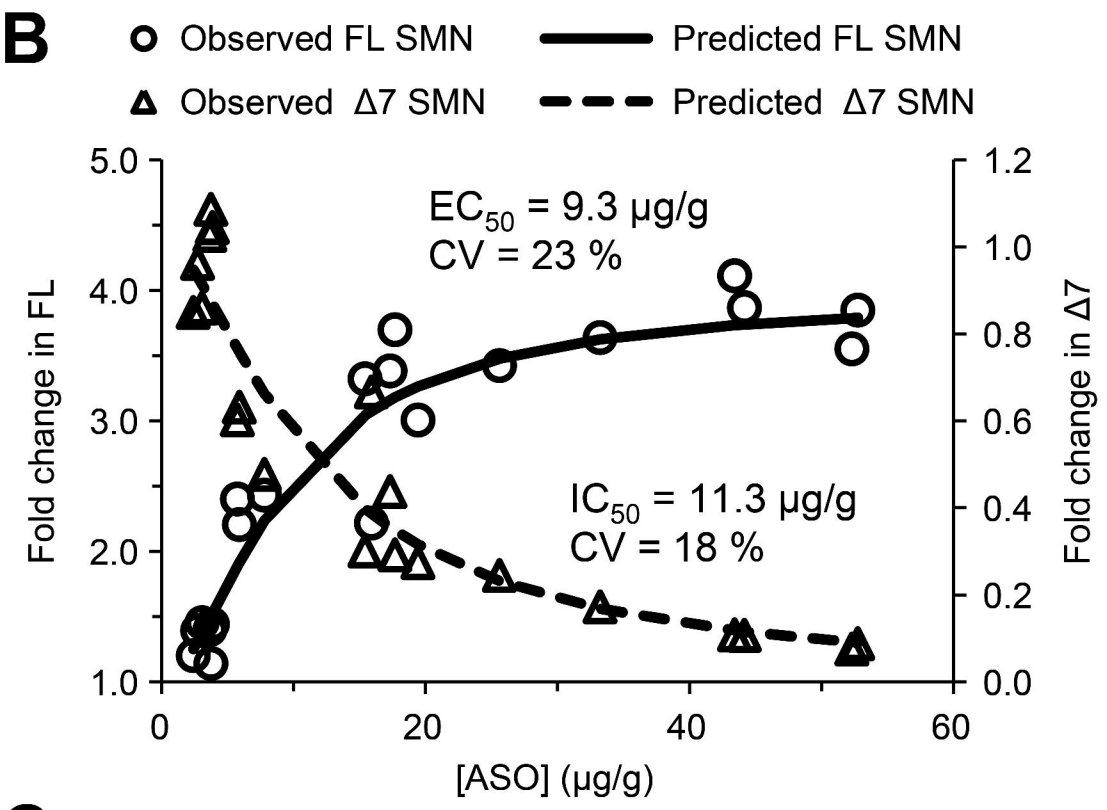

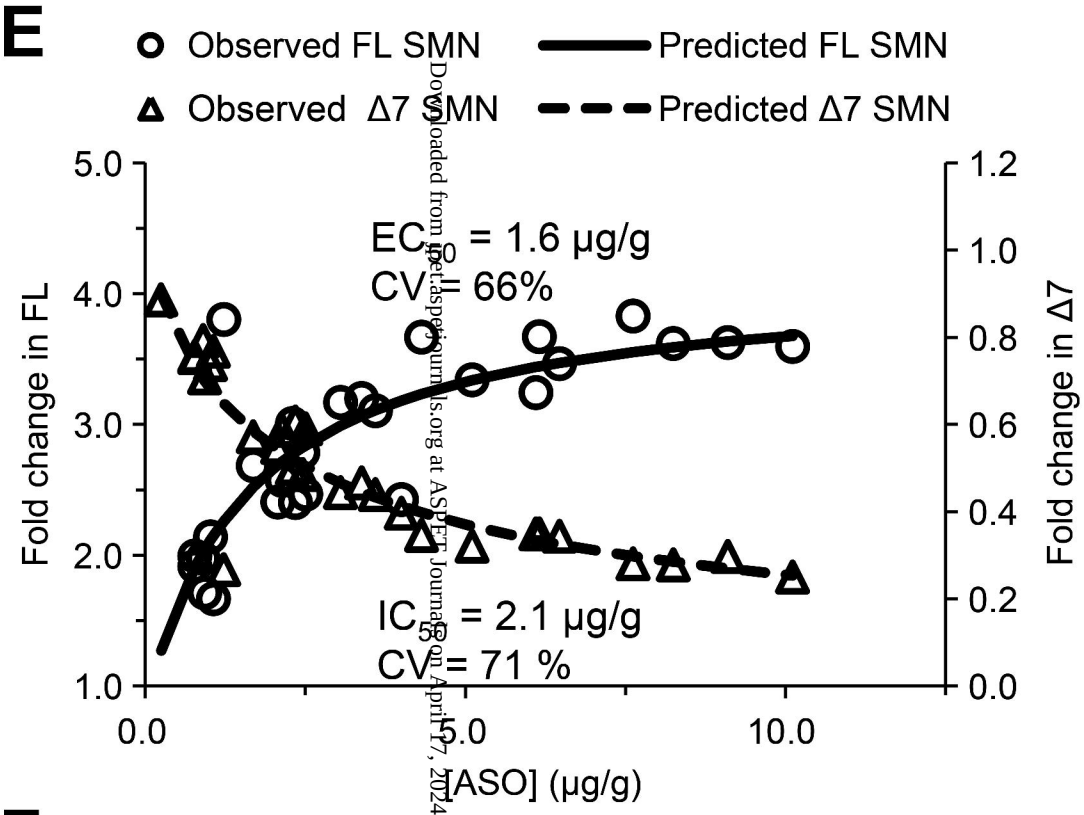

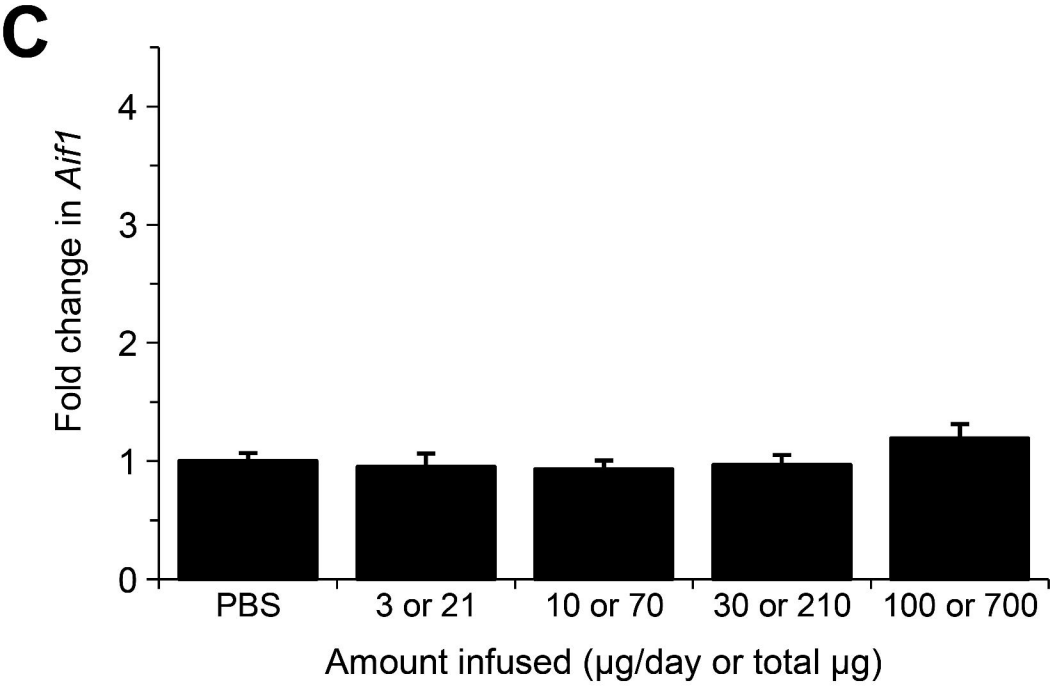

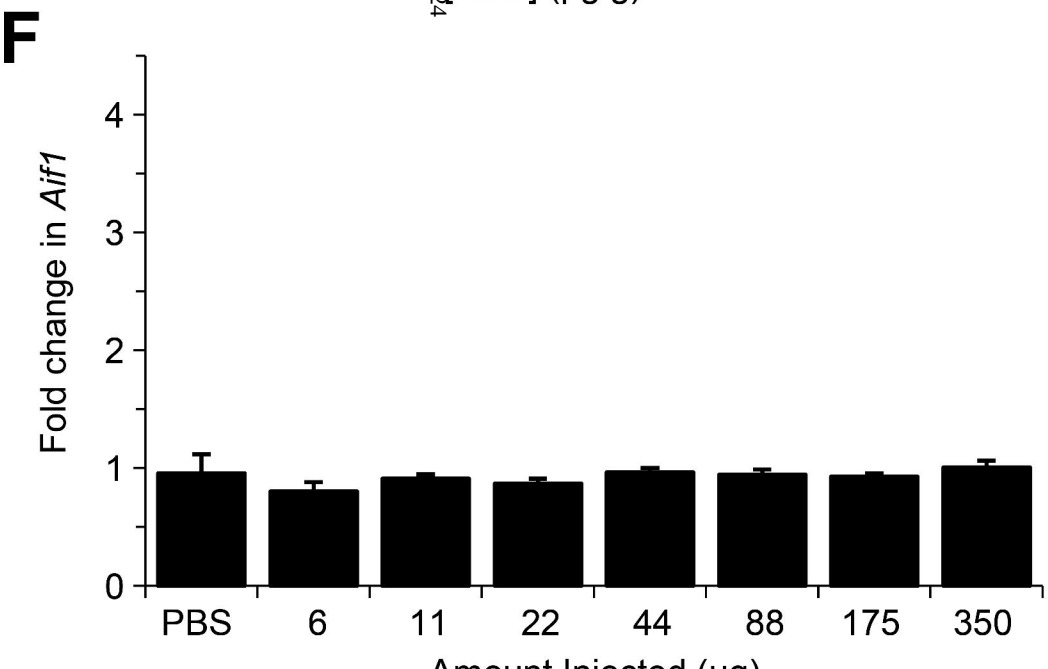

Figure 2

JPET Fast Forward. Published on April 30, 2014 as DOI: 10.1124/jpet.113.206007
This article has not been copyedited and formatted. The final version may differ from this version.

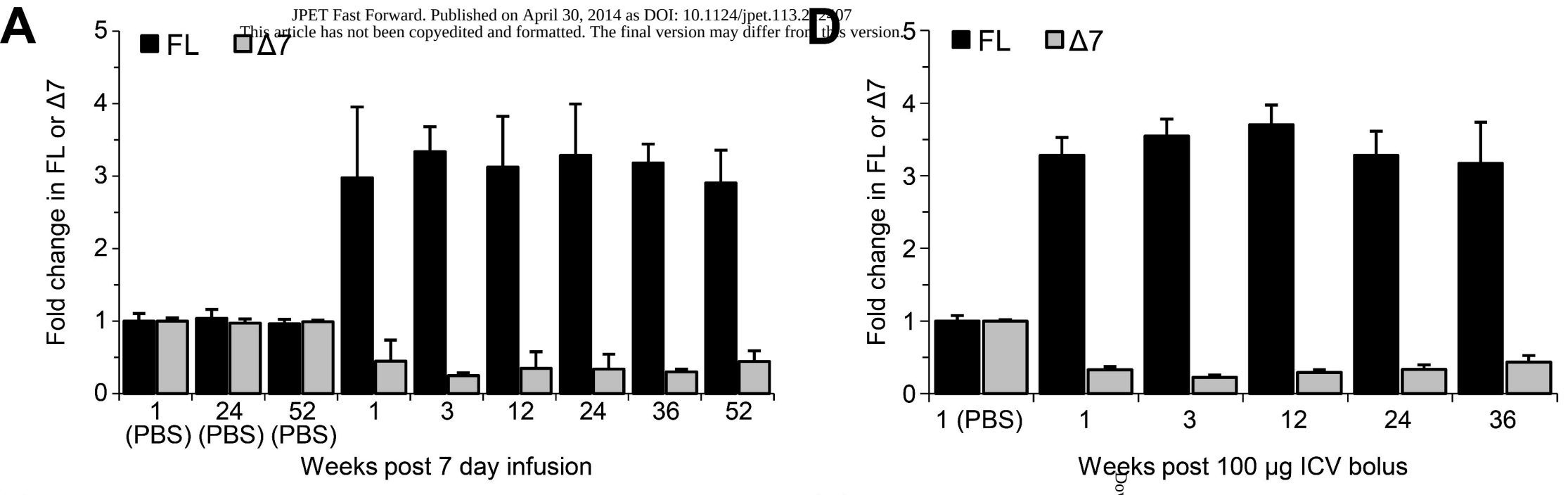

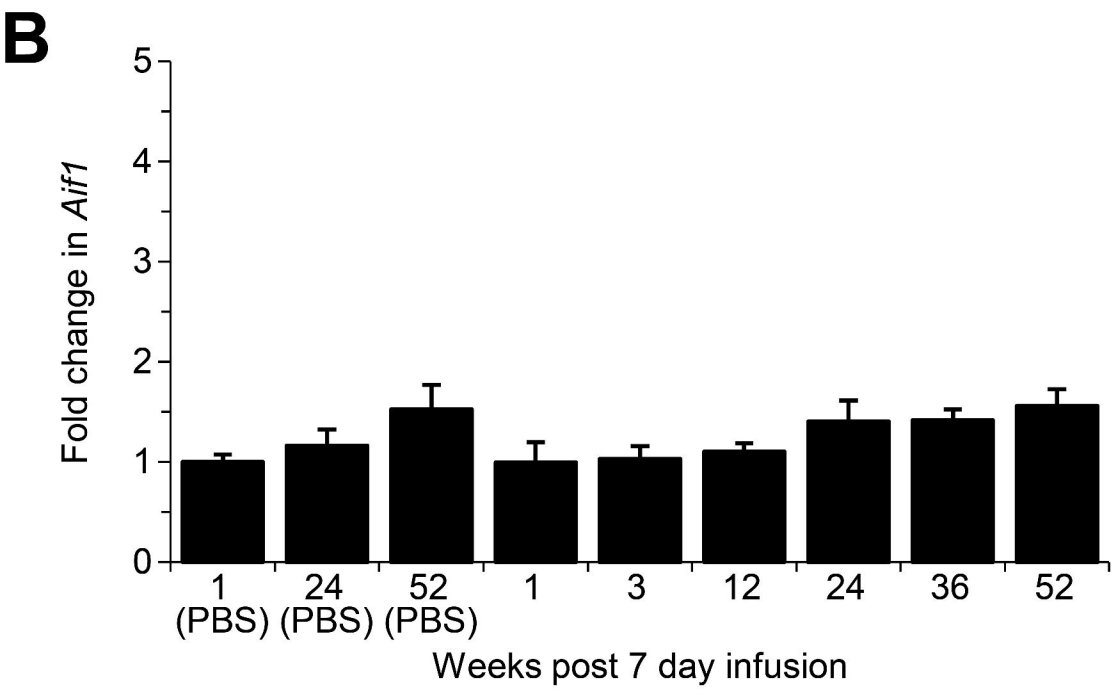

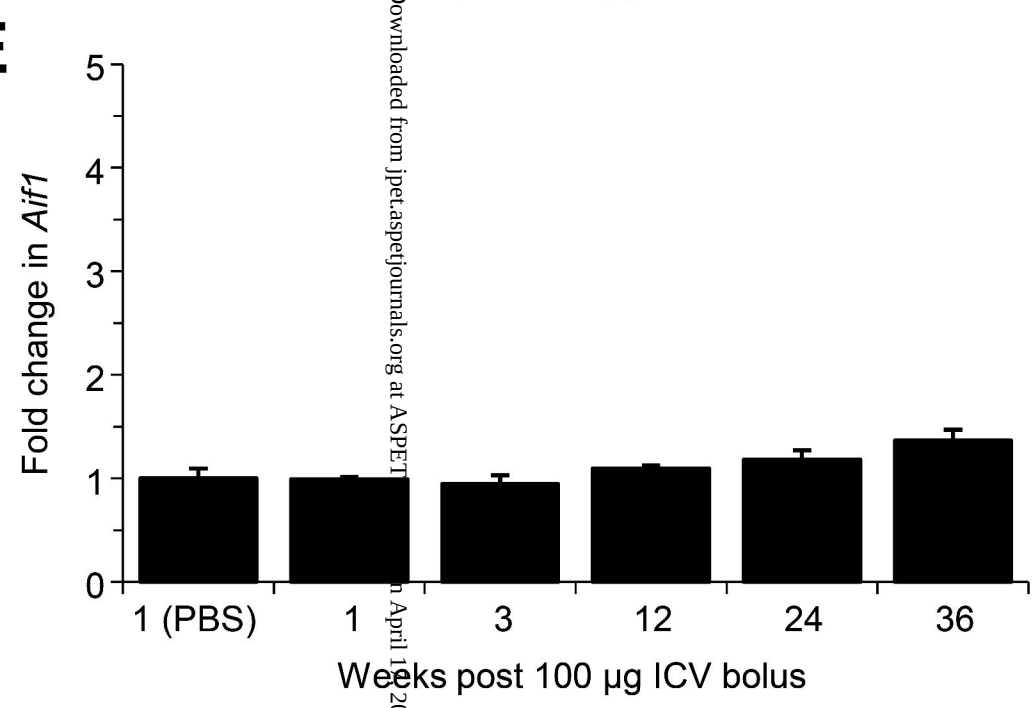

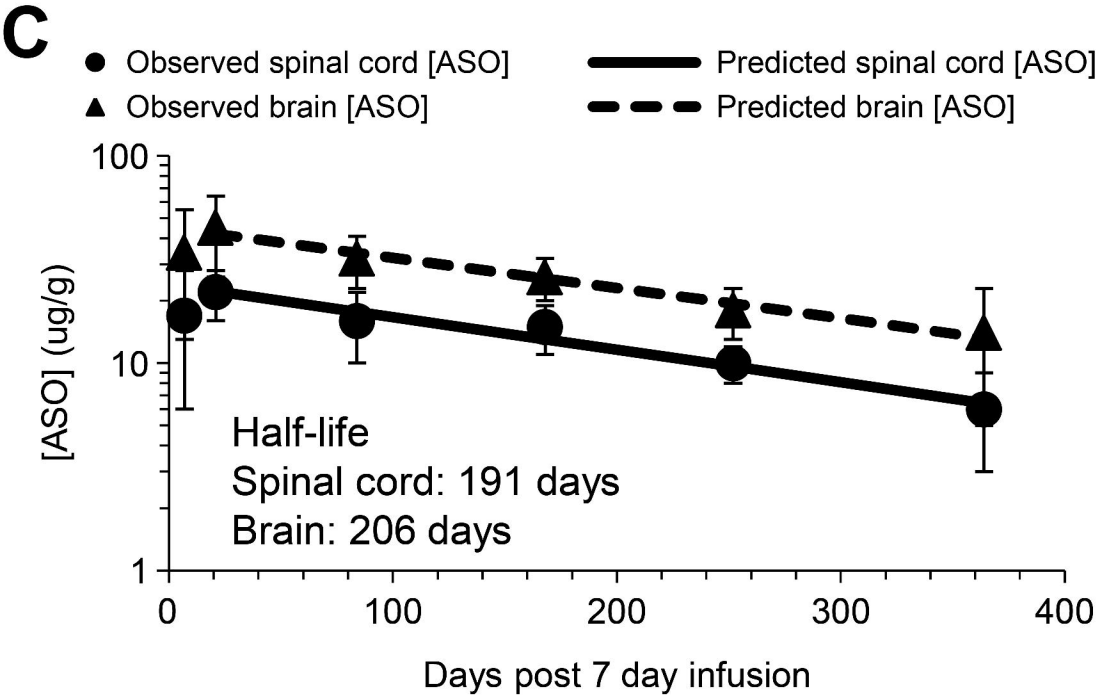

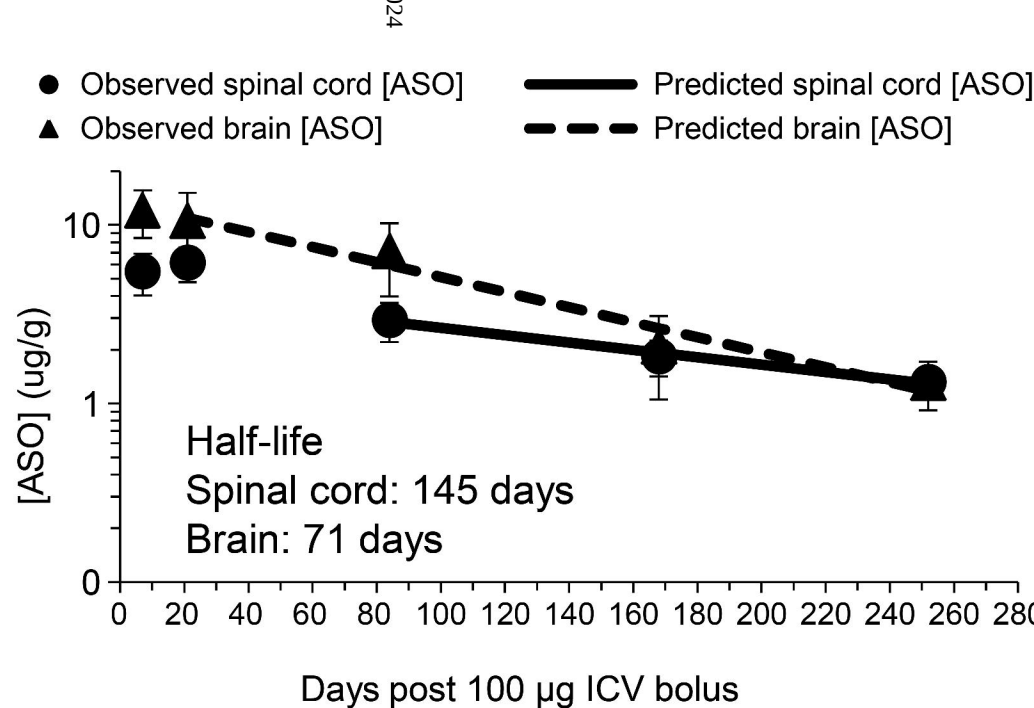

Figure 3

Figure 4

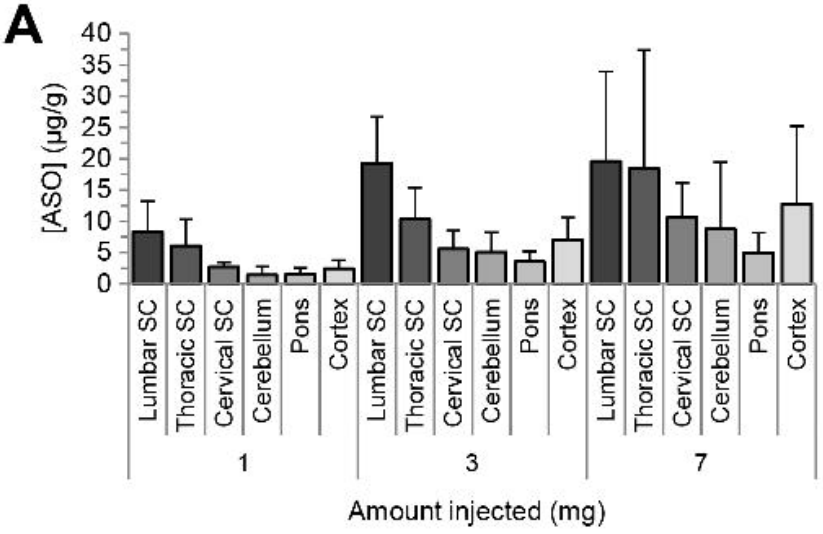
A
[ASO] (µg/g)
40
35
30
25
20
15
10
5
0
Lumbar SC
Thoracic SC
Cervical SC
Cerebellum
Pons
Cortex
1
3
7
Amount injected (mg)

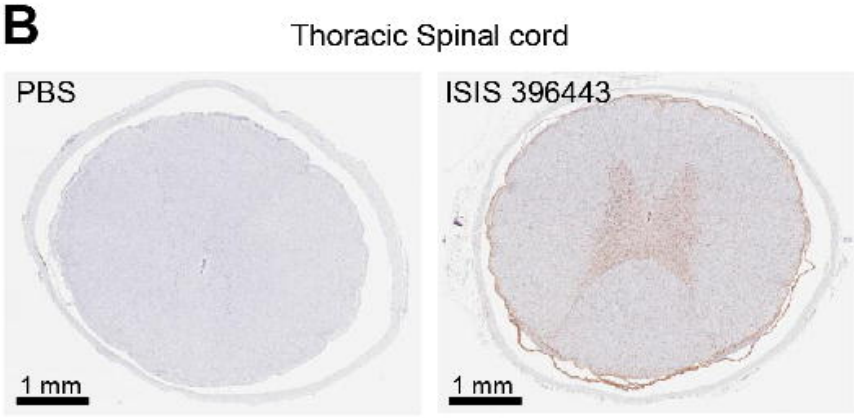
B
Thoracic Spinal cord
PBS
ISIS 396443
1 mm
1 mm

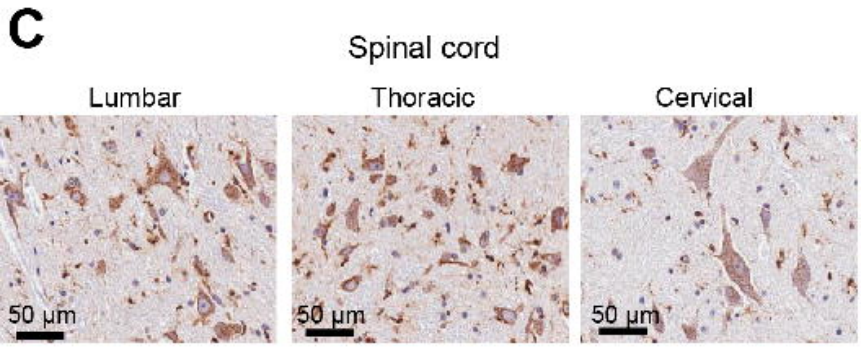
C
Spinal cord
Lumbar
Thoracic
Cervical
50 µm
50 µm
50 µm

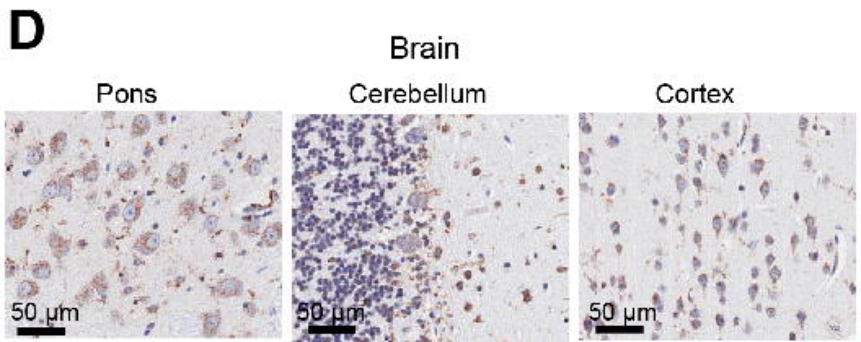
D
Brain
Pons
Cerebellum
Cortex
50 µm
50 µm
50 µm

SUPPLEMENTAL INFORMATION

Pharmacology of a central nervous system delivered 2'-*O*-methoxyethyl-modified survival of motor neuron splicing oligonucleotide in mice and non-human primates

Frank Rigo, Seung J. Chun, Daniel A. Norris, Gene Hung, Sam Lee, John Matson, Robert A. Fey, Hans Gaus, Yimin Hua, John S. Grundy, Adrian R. Krainer, Scott P. Henry and C. Frank Bennett

SUPPLEMENTARY FIGURE LEGENDS

Figure 1 *SMN2* splicing correction in the brain after administration of ISIS 396443 by ICV infusion or ICV bolus injection. (**A**) Real-time RT-PCR analysis of *SMN2* transcripts including exon 7 (FL) or excluding exon 7 (Δ7) in the brain 2 days after the administration of ISIS 396443 by ICV infusion for 7 days at the indicated daily doses. For each dose level n = 5. Error bars represent the s.d. (**B**) For each mouse dosed in **A**, the amount of ISIS 396443 in the brain was measured by HPLC-UV and this was plotted against the level of *SMN2* transcripts including exon 7 (FL) or excluding exon 7 (Δ7) measured in the brain of the same mouse (open circles and triangles, respectively). The calculated EC_{50} and IC_{50} values are shown. (**C**) Same as in **A**, except that the real-time RT-PCR analysis was for *Aif1* transcripts. (**D**) Real-time RT-PCR analysis of *SMN2* transcripts including exon 7 (FL) or excluding exon 7 (Δ7) in the brain 9 days after the administration of ISIS 396443 by ICV bolus injection at the indicated doses. For each dose level n = 4. Error bars represent the s.d. (**E**) Same as in **B**, except that the amount of ISIS 396443 in the brain was measured by HELISA. (**F**) Same as in **D**, except that the real-time RT-PCR analysis was for *Aif1* transcripts. Panels **A** and **C** are reproduced with permission from Hua et al., (Hua et al., 2010) (Copyright 2010, Cold Spring Harbor Laboratory Press).

Figure 2 Distribution of ISIS 396443 and SMN2 protein production in the CNS after a 350 μg ICV bolus injection. Immunohistochemistry with (**A**) a pAb that specifically recognizes the phosphorothioate backbone in ASOs and (**B**) a mAb that is specific for human SMN. Nuclei were counterstained with hematoxylin.

Figure 3 Administration of ISIS 396443 by ICV bolus injection in C/C mice. (**A**) Real-time RT-PCR analysis of *SMN2* transcripts including exon 7 (FL) or excluding exon 7 (Δ7) in the lumbar spinal cord 11 days after the administration of ISIS 396443 by ICV bolus injection at the indicated daily doses. For each dose level n = 4. Error bars represent the s.d. (**B**) For each mouse dosed in **A**, the amount of ISIS 396443 in the thoracic spinal cord was measured by HELISA and this is plotted against the level of *SMN2* transcripts including exon 7 (FL) or excluding exon 7 (Δ7) measured in the lumbar spinal cord of the same mouse (open circles and triangles, respectively). The calculated EC_{50} and IC_{50} values are shown. (**C**) Same as in **A**, except that the real-time RT-PCR analysis was for *Aif1* transcripts. (**D**) Real-time RT-PCR analysis of *SMN2* transcripts including exon 7 (FL) or excluding exon 7 (Δ7) in the brain 11 days after the administration of ISIS 396443 by ICV bolus injection at the indicated doses. For each dose level n = 4. Error bars represent the s.d. (**E**) Same as in **B**, except that the amount of ISIS 396443 in the brain was measured by HELISA. (**F**) Same as in **D**, except that the real-time RT-PCR analysis was for *Aif1* transcripts.

Figure 4 Administration of ISIS 396443 by IP bolus injection. (**A**) Real-time RT-PCR analysis of *SMN2* transcripts including exon 7 (FL) or excluding exon 7 (Δ7) in the liver after the administration of ISIS 396443 at the indicated dose by IP injection. Mice were dosed every 2 days for a total of 4 doses and were euthanized 48 h after the last dose. For each dose level n = 6. Error bars represent the s.d. (**B**) For each mouse dosed in **A**, the amount of ISIS 396443 in the liver was measured by CGE-UV and this was plotted against the level of *SMN2* transcripts including exon 7 (FL) or excluding exon 7 (Δ7) measured in the liver of the same mouse (open circles and triangles, respectively). The calculated EC_{50} and IC_{50} values are shown. (**D**) Body weight, (**E**) organ weights, (**F**) ALT and AST, and (**G**) BUN were measured after mice were euthanized. n = 6 and error bars represent the s.d.

Figure 5 Duration of action in the brain after ICV infusion or ICV bolus injection of ISIS 396443. (**A**) Real-time RT-PCR analysis of *SMN2* transcripts including exon 7 (FL) or excluding exon 7 (Δ7) in the

brain at the indicated time points after the administration of ISIS 396443 by ICV infusion at 50 μg/day for 7 days. PBS, n = 4; 1 and 3 weeks, n = 5; 12 week, n = 6; 24 week n = 7; 36 week, n = 6; 52 week n = 7. Error bars represent the s.d. (**B**) Same as in **A**, except that the real-time RT-PCR analysis was for *Aif1* transcripts. (**C**) Real-time RT-PCR analysis of *SMN2* transcripts including exon 7 (FL) or excluding exon 7 (Δ7) in the brain at the indicated time points after the administration of 100 μg of ISIS 396443 by ICV bolus injection. For each time point n = 5, except for the 24 week group where n = 4. Error bars represent the s.d. (**D**) Same as in **C**, except that the real-time RT-PCR analysis was for *Aif1* transcripts.

Figure 6 Duration of action in the spinal cord and brain after a 25 μg ICV bolus injection of ISIS 396443. (**A**) Real-time RT-PCR analysis of *SMN2* transcripts including exon 7 (FL) or excluding exon 7 (Δ7) in the lumbar spinal cord at the indicated time points after the administration of 25 μg of ISIS 396443 by ICV bolus injection. For each time point n = 5, except for the 24 week group where n = 4. Error bars represent the s.d. (**B**) Same as in **A**, except that the real-time RT-PCR analysis was for *Aif1* transcripts. (**C**) Same as in **A**, except that real-time RT-PCR analysis was done with transcripts form the brain. (**D**) Same as in **C**, except that the real-time RT-PCR analysis was for *Aif1* transcripts. (**E**) The amount of ISIS 396443 in the thoracic spinal cord and brain was measured by HELISA. For each time point n = 5, except for the 12 week group where n = 4. Error bars represent the s.d. The calculated tissue half-life of ISIS 396443 is shown.

Figure 7. Distribution of ISIS 396443 and SMN2 protein production in the spinal cord 36 and 52 weeks after a 7 day infusion of 50 μg/day. Immunohistochemistry with (**A**) a pAb that specifically recognizes the phosphorothioate backbone in ASOs and (**B**) a mAb that is specific for human SMN. Nuclei were counterstained with hematoxylin.

Figure 8. Distribution of ISIS 396443 and SMN2 protein production in the spinal cord at various time points after a 100 or 25 μg ICV bolus injection. Immunohistochemistry with (**A**) a pAb that specifically recognizes the phosphorothioate backbone in ASOs and (**B**) a mAb that is specific for human SMN. Nuclei were counterstained with hematoxylin.

Figure 9 Duration of action in the liver after administration of ISIS 396443 by IP injection. (**A**) Radioactive RT-PCR analysis of *SMN2* transcripts including exon 7 in the liver at the indicated time points after administration of 50 mg/kg of ISIS 396443 every 2 days for a total of 4 doses by IP injection. For each dose level n = 5. Error bars represent the s.d. (**B**) The amount of ISIS 396443 in the liver was measured at each time point by HPLC-MS/MS. For each time point n = 5. Error bars represent the s.d. The calculated tissue half-life of ISIS 396443 is shown.

Figure 10 Administration of an ISIS 396443 decoy after ISIS 396443-mediated correction of *SMN2* splicing. (**A**) Real-time RT-PCR analysis of *SMN2* transcripts including exon 7 (FL) or excluding exon 7 (Δ7) in the lumbar spinal cord after administration with a single ICV bolus injection of 100 μg ISIS 396443 (443) and after 3 weeks followed by 400 μg of the decoy (α443). Mice were euthanized 2 weeks after the administration of α443. For each group n = 5. Error bars represent the s.d. (**B**) Same as in **a** except that RNA was isolated from the brain. (**C, D**) Same as in **A** and **B**, respectively, except that 25 μg of 443 and 100 μg α443 were administered. Mice were euthanized 2 and 4 weeks after the administration of α443.

Figure 11 Evaluation of ISIS 396443, 2'-OMe, PMO and cEt/MOE ASOs in fibroblasts from SMA patients. (**A**) Real-time RT-PCR analysis of *SMN2* transcripts including exon 7 (left panel) or

excluding exon 7 (right panel) isolated after transfecting SMA patient fibroblasts with increasing concentrations of ISIS 396443 (2'-MOE) or the 2'-OMe ASO. Error bars represent the s.d. (**B, C**) Same as in **A** except that ASOs were transfected by electroporation. For **B** and **C** error bars represent the s.d. of quadruplicate samples.

Figure 12 Comparison of ISIS 396443 to the 2'-MOE ASO in the brain. (**A**) Real-time RT-PCR analysis of *SMN2* transcripts including exon 7 (FL) or excluding exon 7 (Δ7) in the brain, 9 days after the administration of ISIS 396443 or the 2'-OMe ASO by ICV bolus injection at the indicated doses. For each dose level n = 4. Error bars represent the s.d. (**B**) The amount of ISIS 396443 and the 2'-OMe ASO in the brain of each mouse were measured by HELISA. For each dose level n=4. Error bars represent the s.d. (**C**) Same as in **A**, except that the real-time RT-PCR analysis was for *Aif1* transcripts. (**D**) Same as in **Fig. 3B** except that the real-time RT-PCR analysis was for *Aif1* transcripts.

Figure 13 ISIS 396443 PK/PD relationship in the spinal cord after ICV bolus injection. For each mouse dosed in **Fig. 3D**, the amount of ISIS 396443 in the thoracic spinal cord was measured by HELISA and this is plotted against the level of *SMN2* transcripts including exon 7 (FL) or excluding exon 7 (Δ7) measured in the lumbar spinal cord of the same mouse (open circles and triangles, respectively). The calculated EC_{50} and IC_{50} values are shown.

Figure 14 Comparison of ISIS 396443 to the PMO-20 ASO in the brain. (**A**) Real-time RT-PCR analysis of transcripts including exon 7 (FL) or excluding exon 7 (Δ7) in the brain, 7 days after the administration of ISIS 396443 or the PMO-20 ASO by ICV bolus injection at the indicated doses. For each dose level n=4. Error bars represent the s.d. (**B**) The amount of ISIS 396443 and the PMO-20 ASO in the brain of each mouse were measured by HELISA. For each dose level n=4. Error bars represent the s.d. The concentration of (**C**) ISIS 396443 and (**D**) the PMO-20 ASO in the thoracic spinal cord of each mouse in **B** was plotted against the level of *SMN2* transcripts including exon 7 (FL) or excluding exon 7 (Δ7) measured in the brain of the same mouse (open circles and triangles, respectively). The calculated EC_{50} and IC_{50} values are shown.

Figure 15 Comparison of ISIS 396443 to the PMO-23 ASO in the CNS. (**A**) Real-time RT-PCR analysis of transcripts including exon 7 (FL) or excluding exon 7 (Δ7) in the lumbar spinal cord, 7 days after the administration of ISIS 396443 or the PMO-23 ASO by ICV bolus injection at the indicated doses. For each dose level n=4. Error bars represent the s.d. (**B**) Same as in **A**, except that the real-time RT-PCR analysis was for *Aif1* transcripts. (**C, D**) Same as in **A**, **B** except that the real-time RT-PCR analysis was for transcripts isolated from the brain.

Figure 16 Comparison of ISIS 396443 to the cEt/MOE ASO in the brain. Real-time RT-PCR analysis of *SMN2* transcripts including exon 7 (FL) or excluding exon 7 (Δ7) in the brain 9 days after the administration of ISIS 396443 or the cEt/MOE ASO by ICV bolus injection at the indicated doses. For each dose level n = 4. Error bars represent the s.d.

Figure 17 Analysis of *SMN* splicing in non-human primates. (**A**) Semi-quantitative RT-PCR analysis of *SMN* transcripts in rhesus monkey cells after ASO transfection. (**B**) Semi-quantitative RT-PCR analysis of *SMN* transcripts in the spinal cord of cynomolgus monkeys.

Table 1 List of chemically modified ASOs.

Table 2 List of List of primers.

Supplemental Figure 1

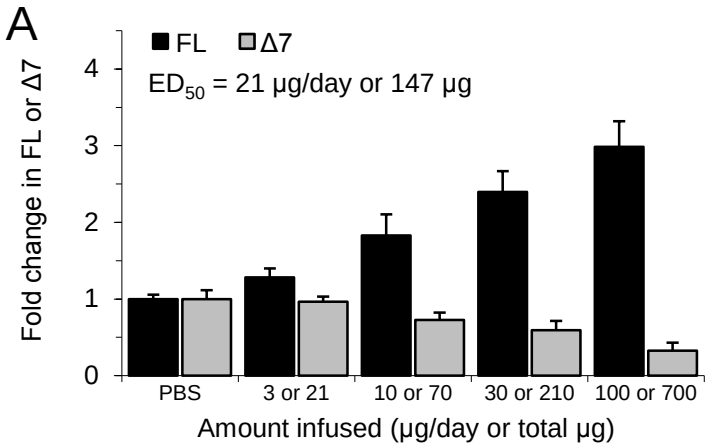

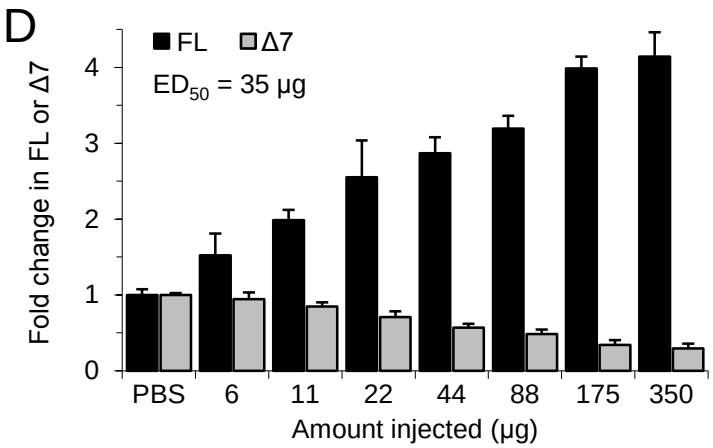

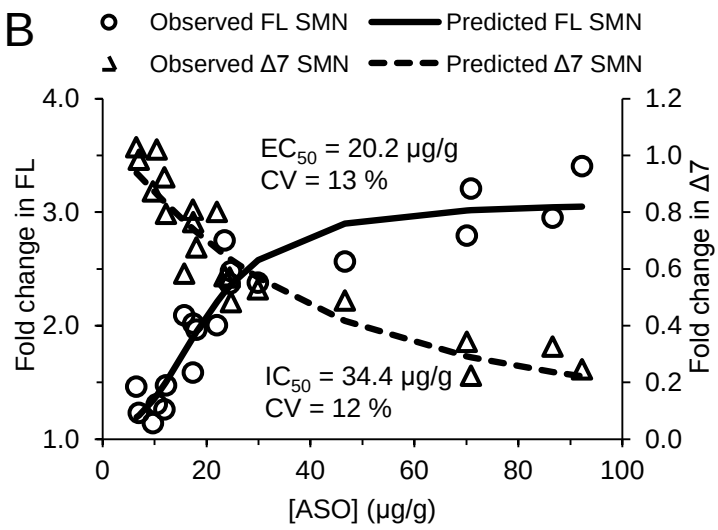

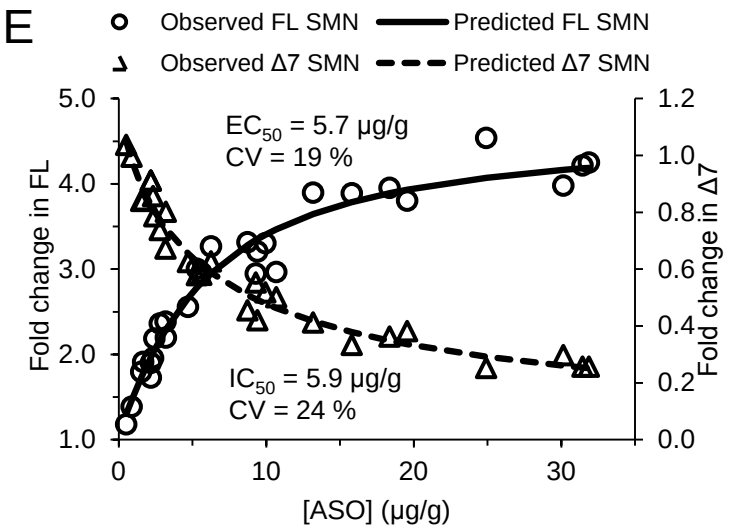

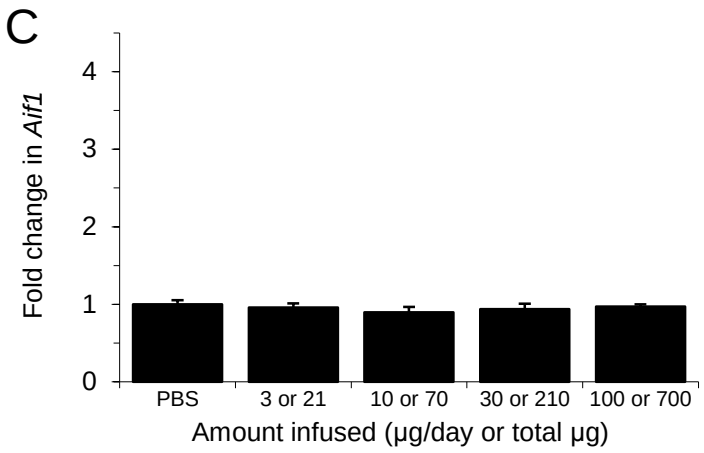

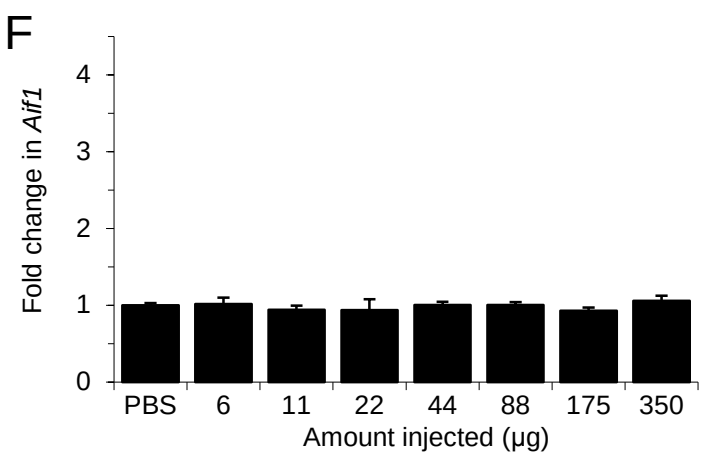

Supplemental Figure 2

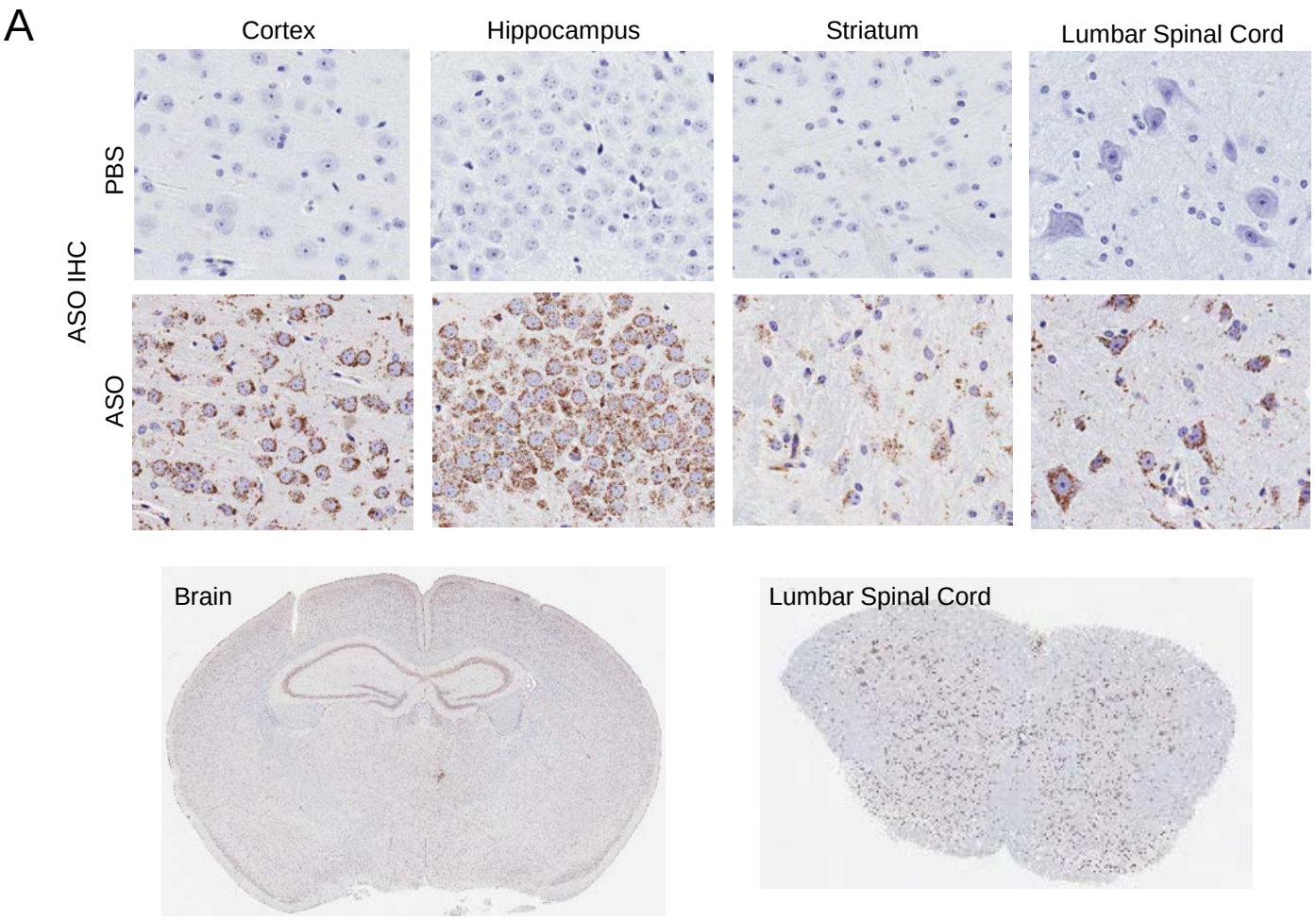

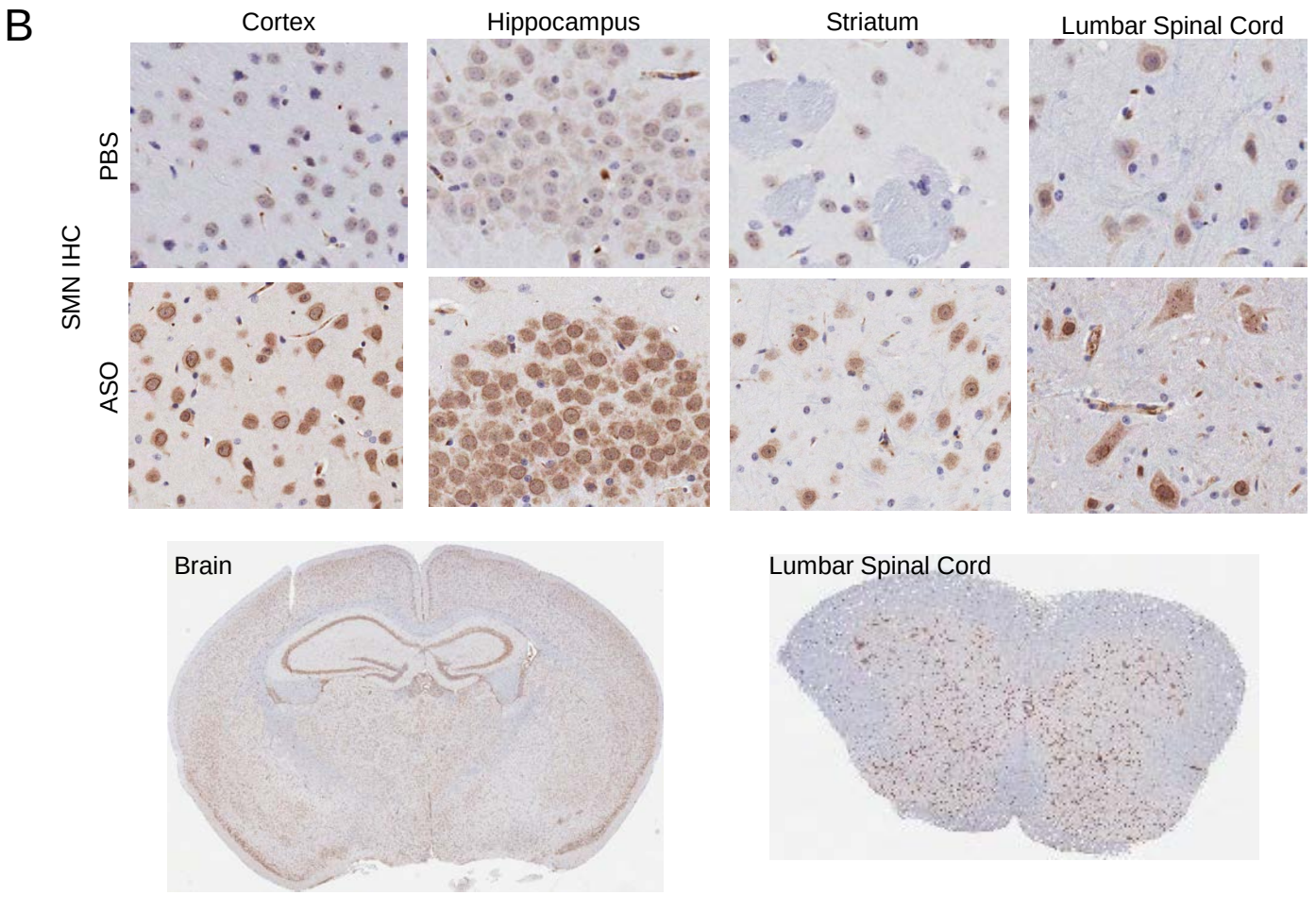

Supplemental Figure 3

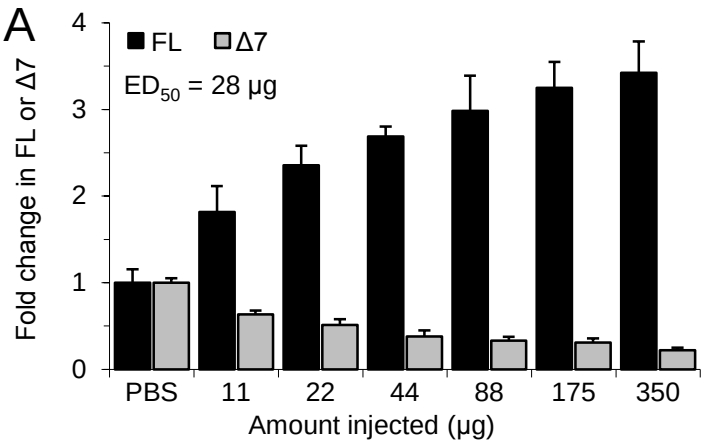

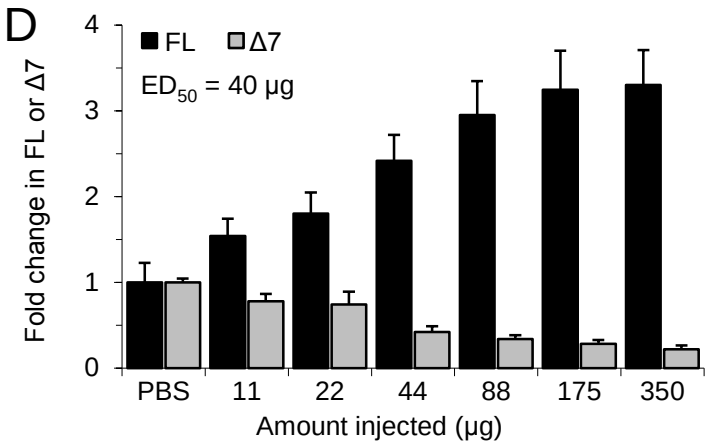

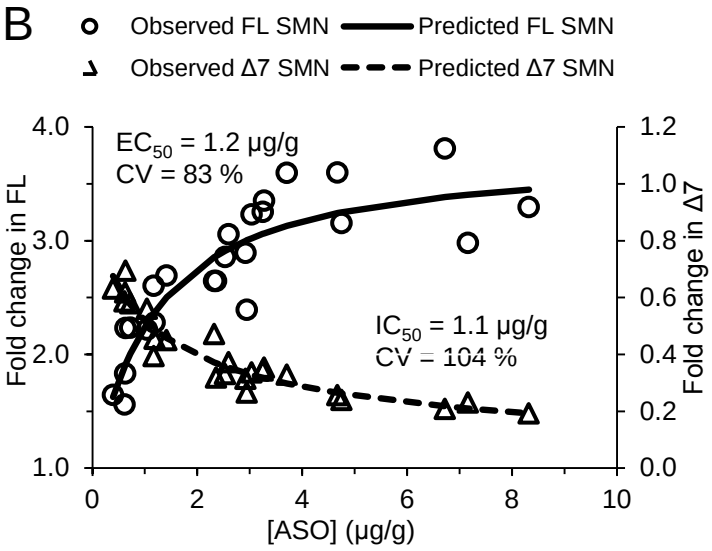

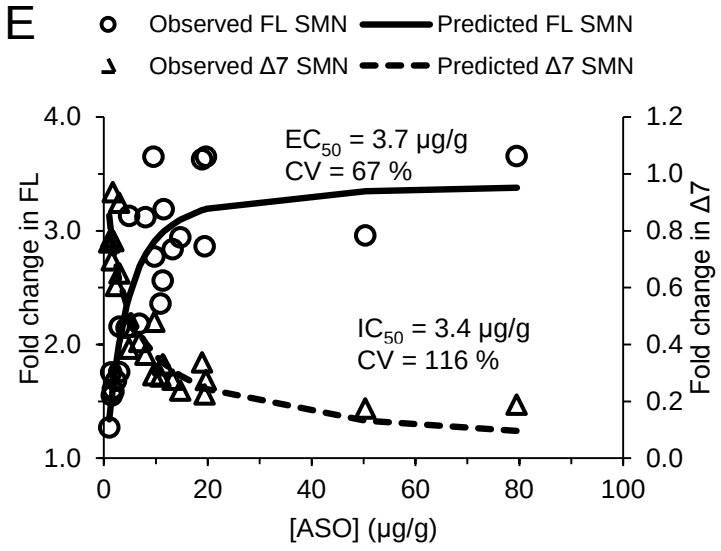

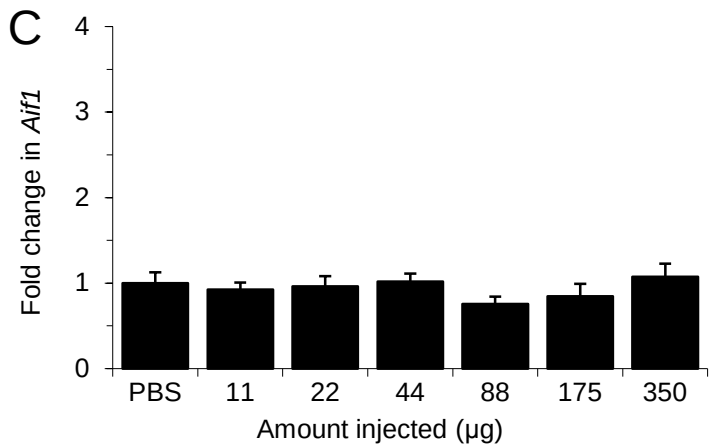

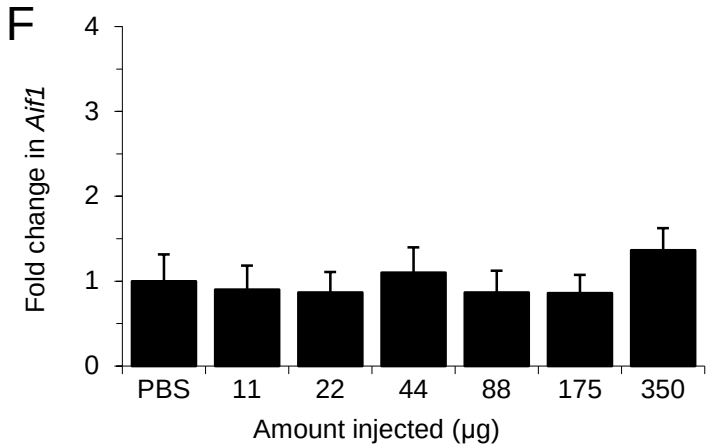

Supplemental Figure 4

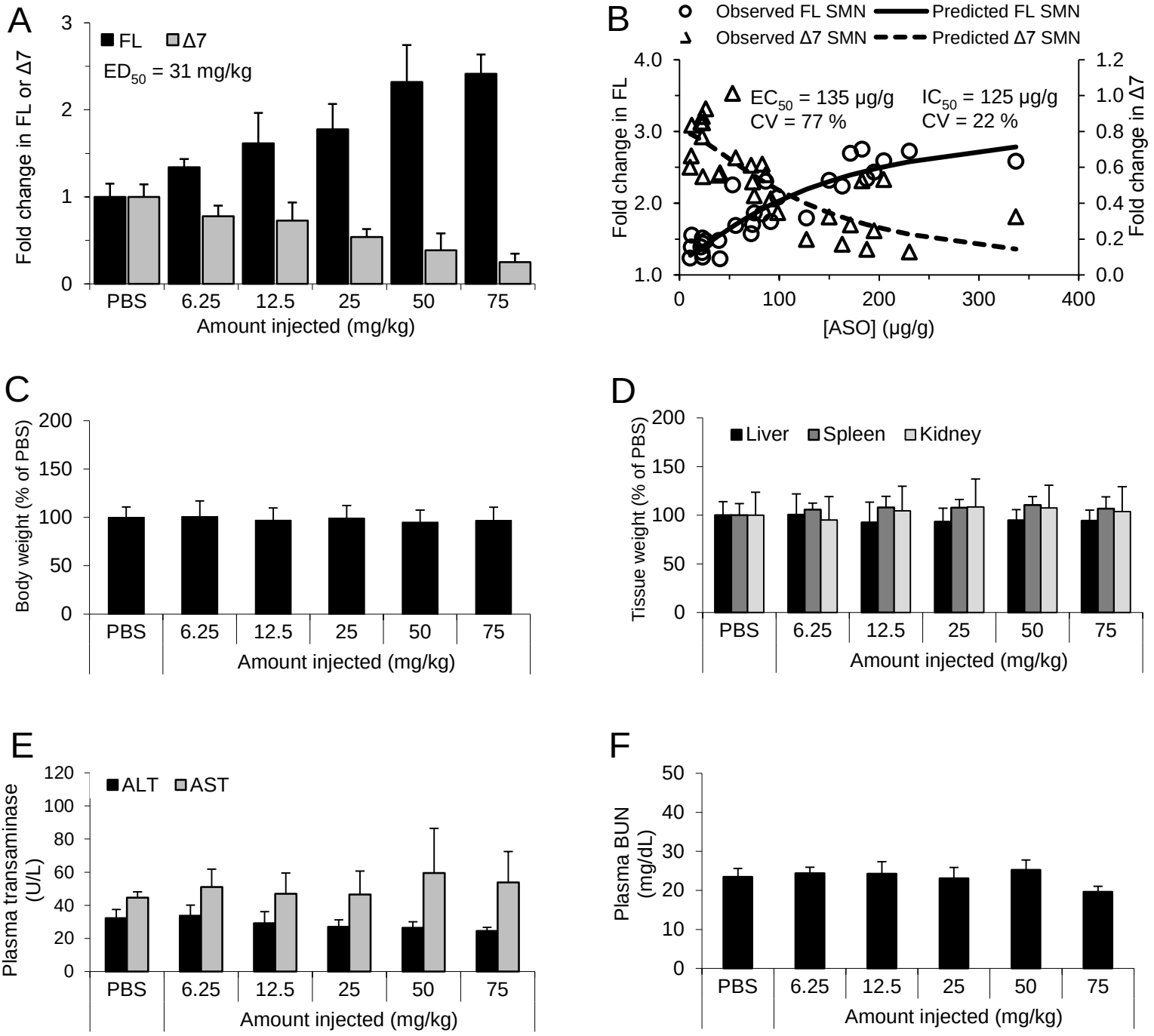

Supplemental Figure 5

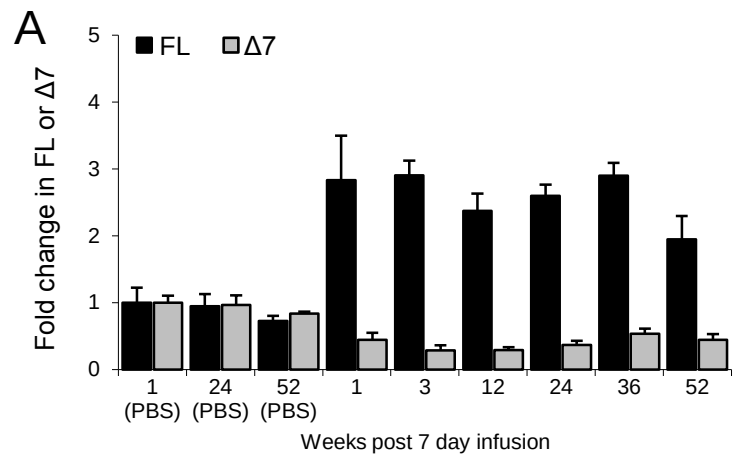

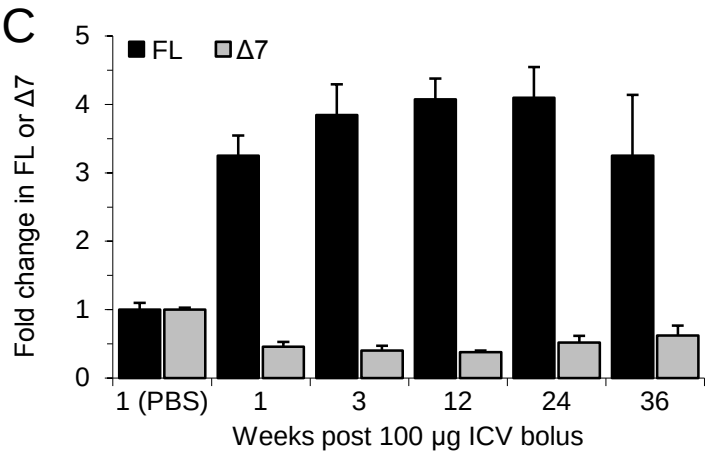

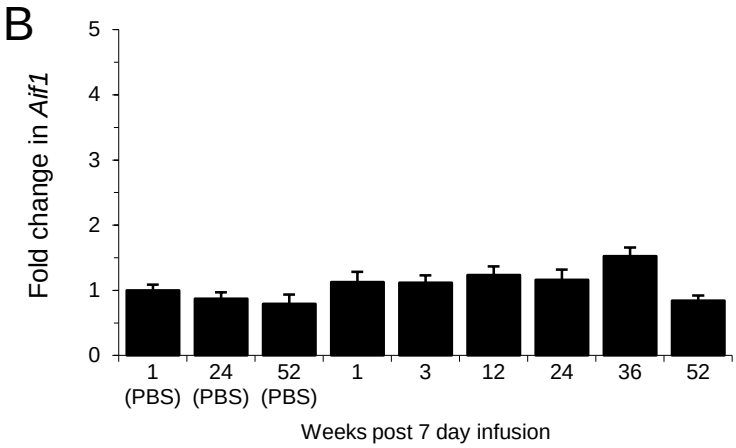

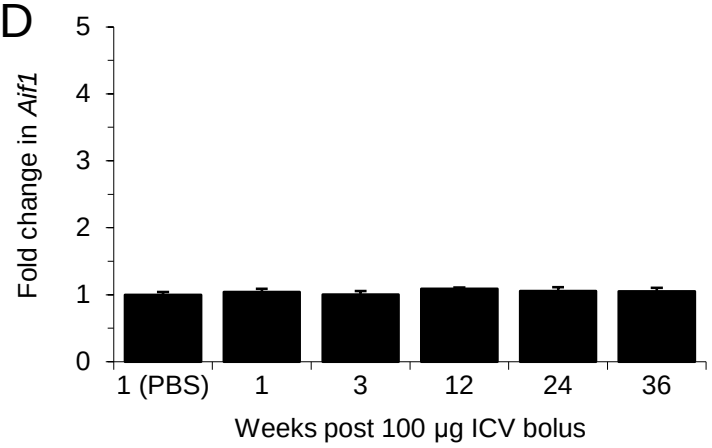

Supplemental Figure 6

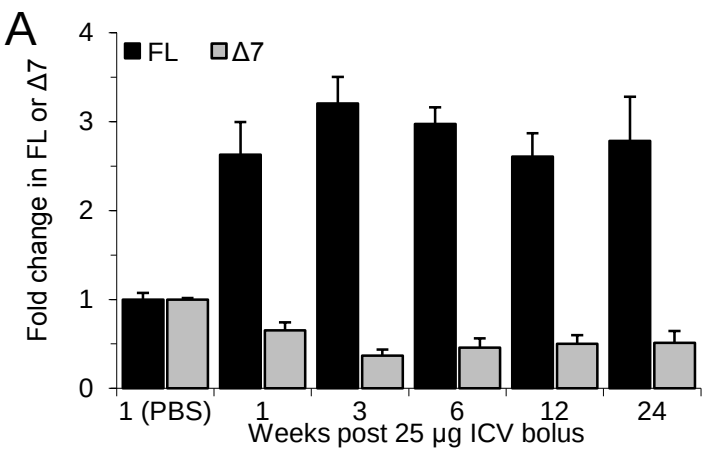

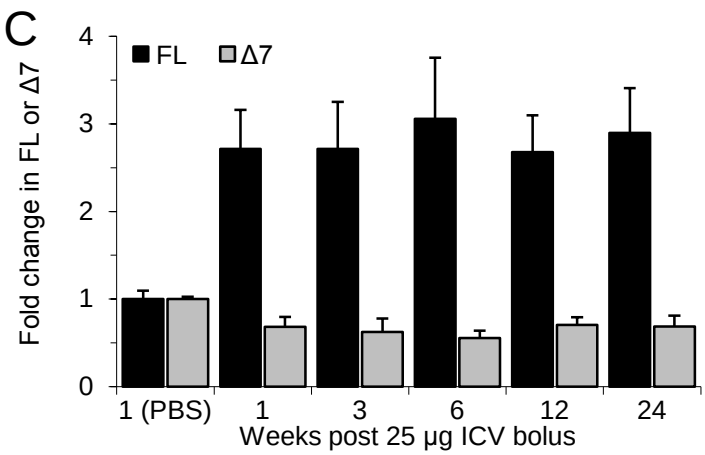

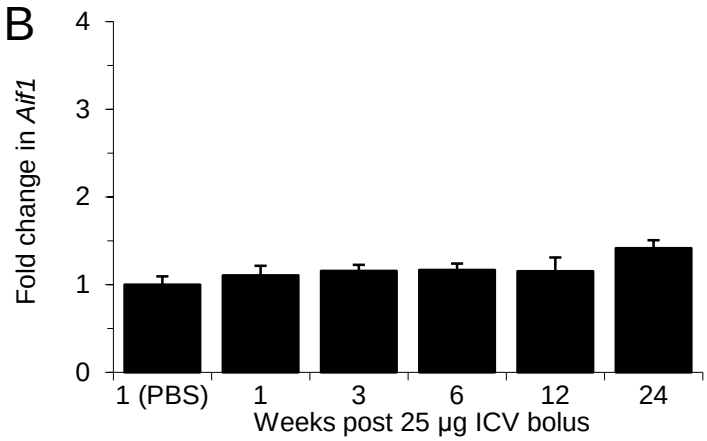

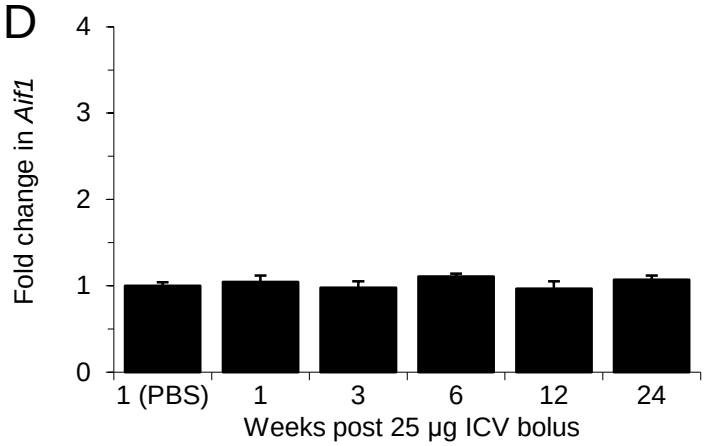

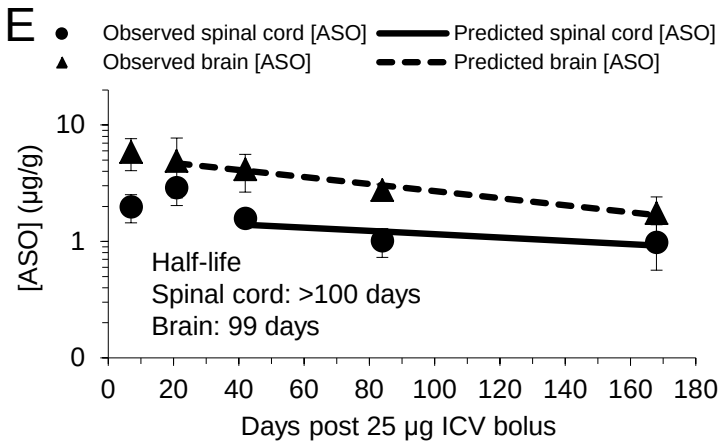

Supplemental Figure 7

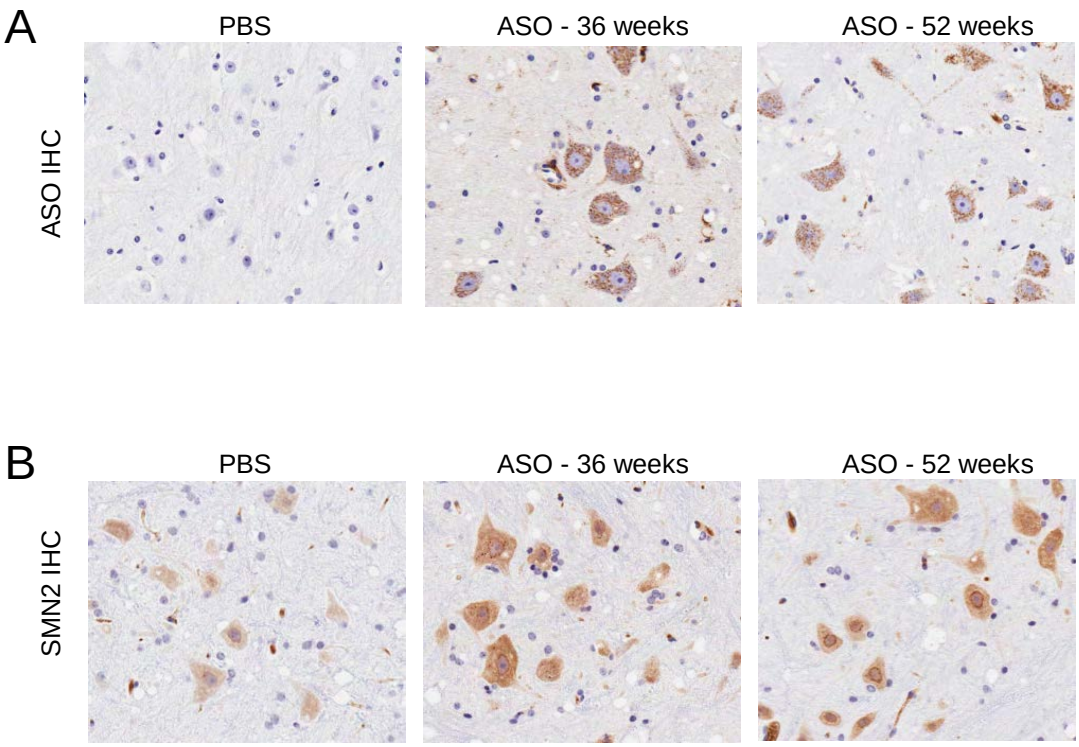

Supplemental Figure 8

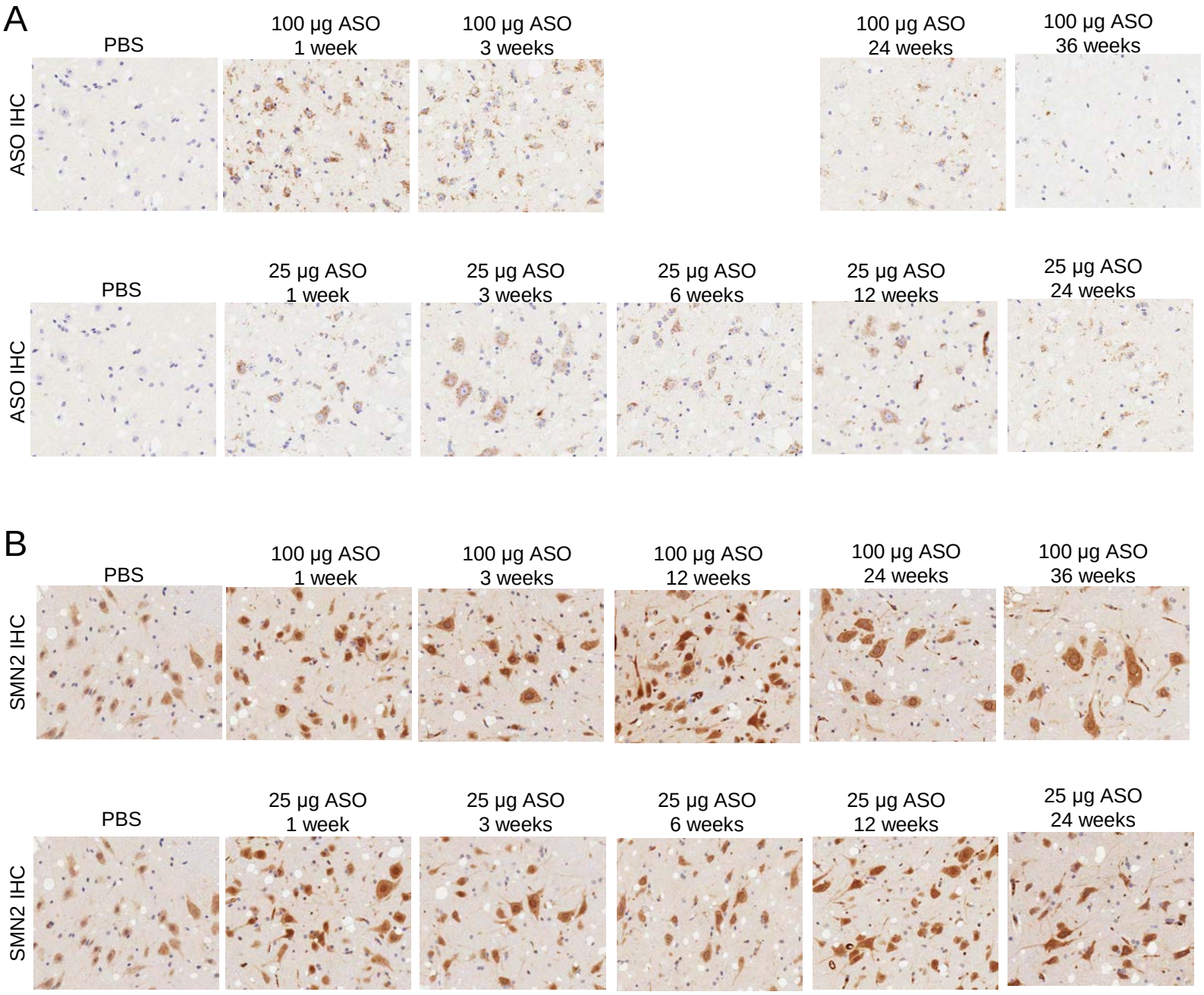

Supplemental Figure 9

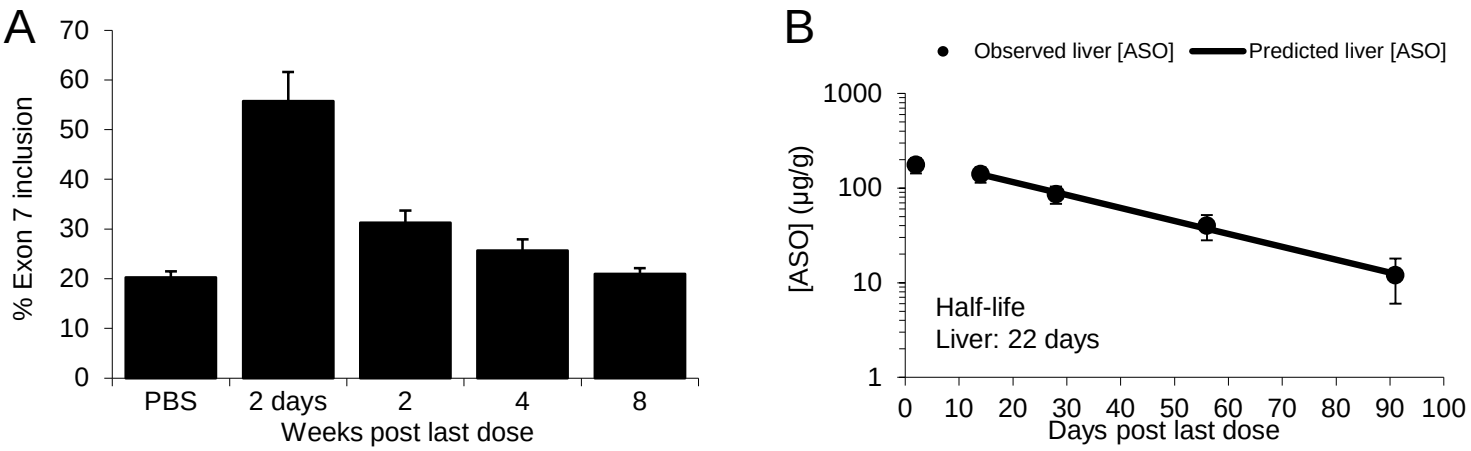

Supplemental Figure 10

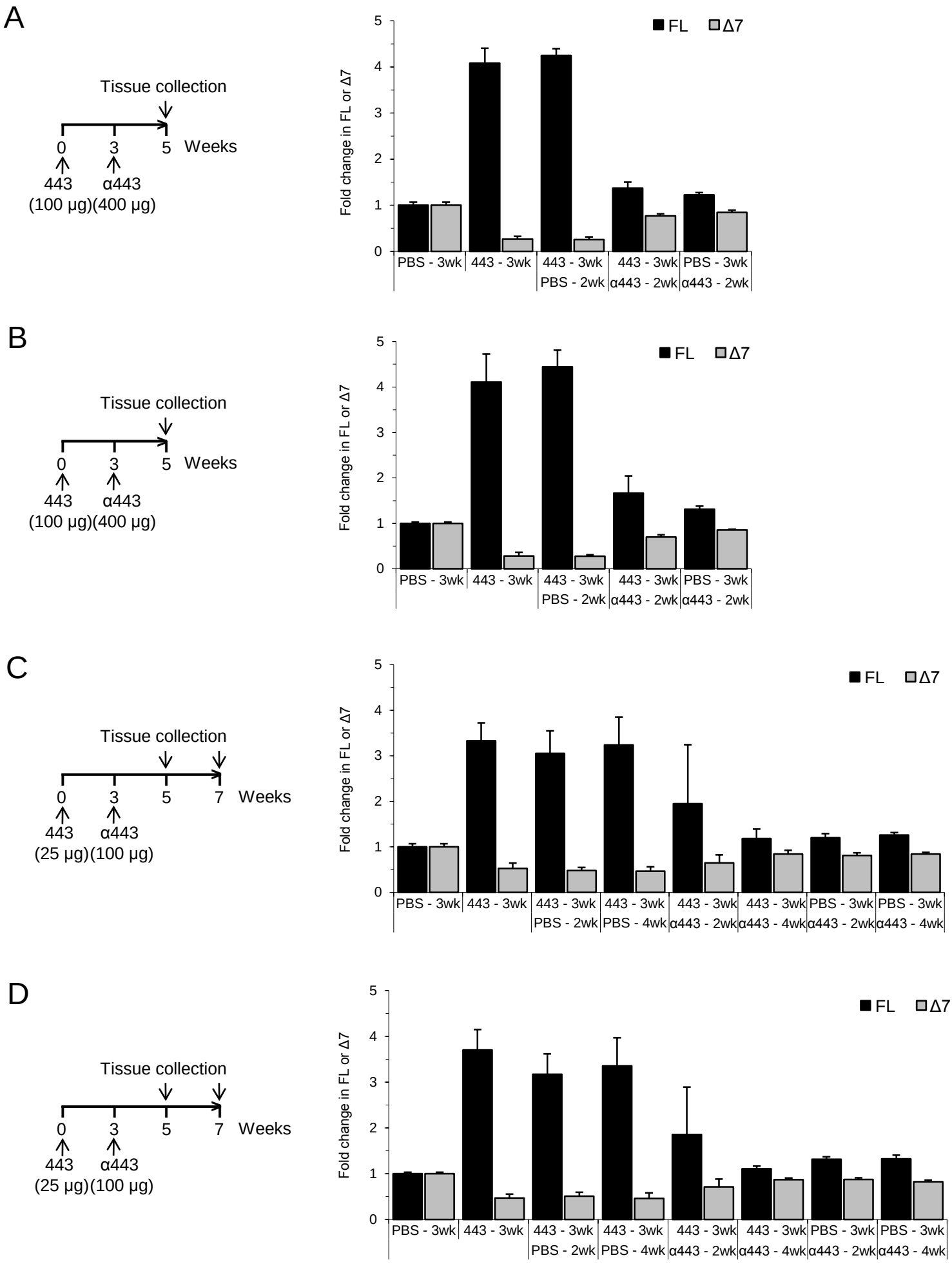

Supplemental Figure 11

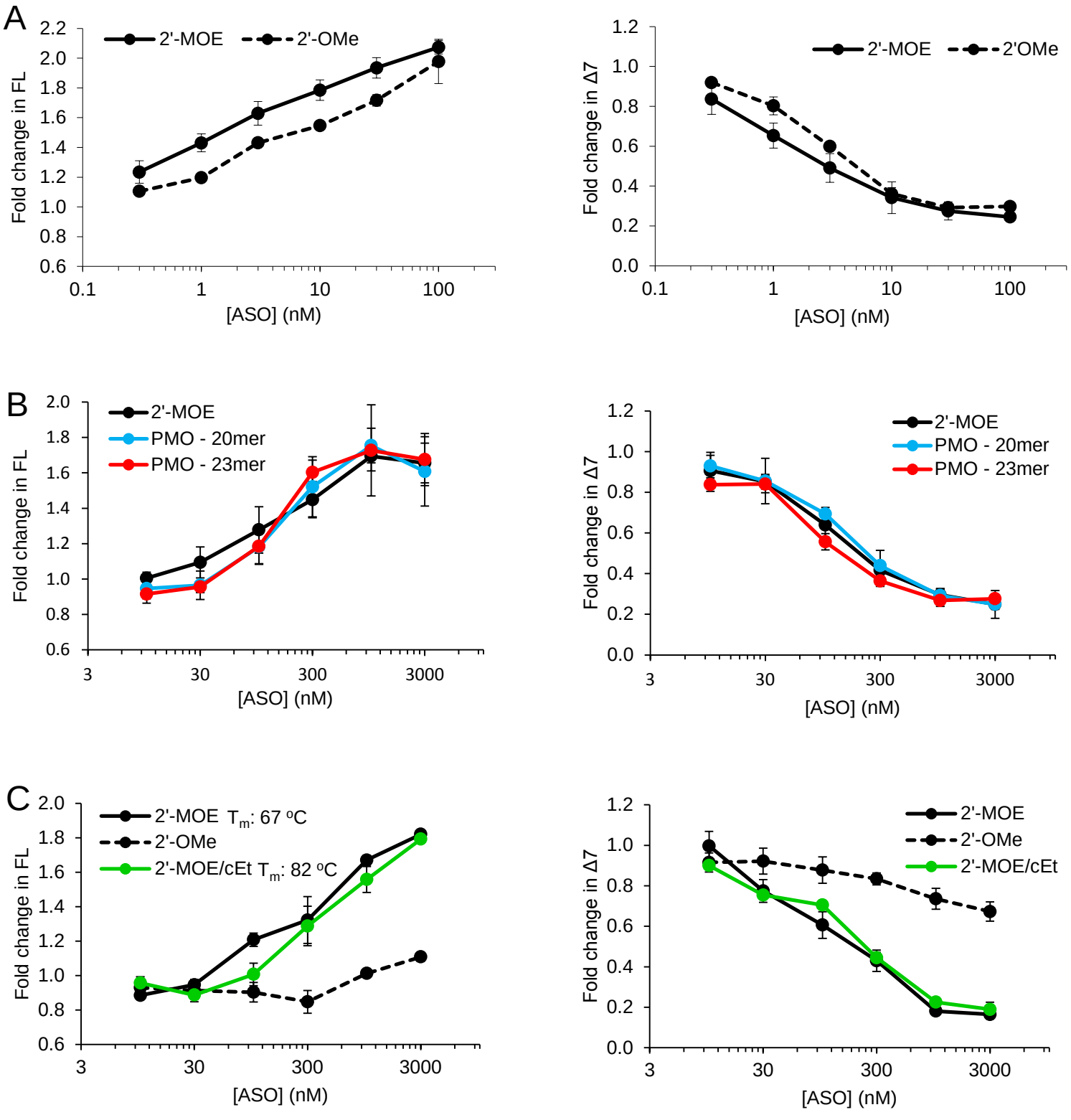

Supplemental Figure 12

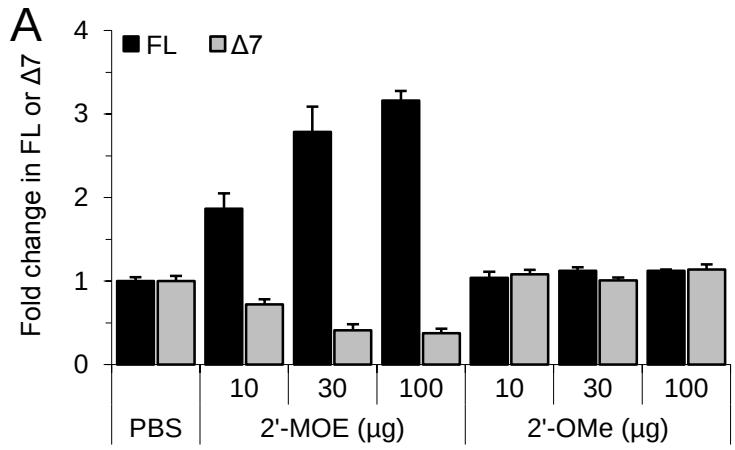

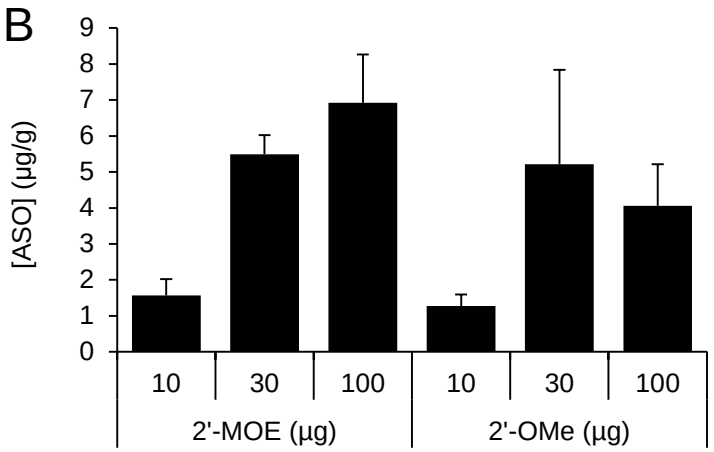

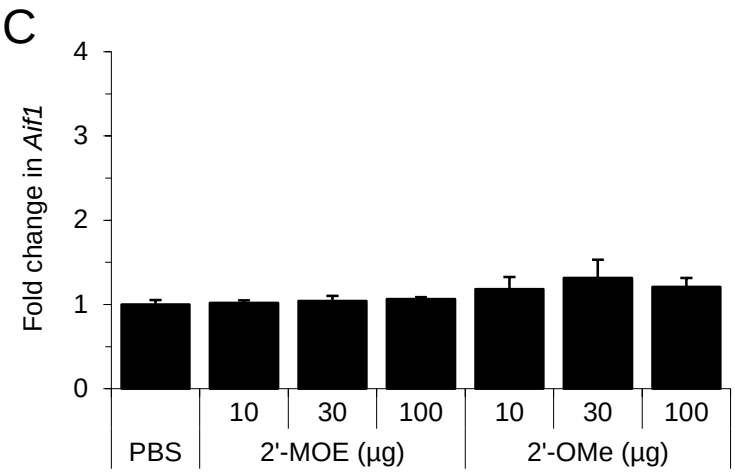

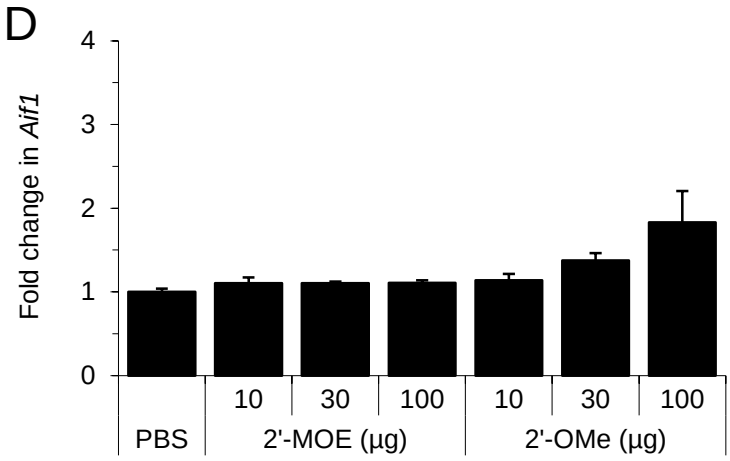

Supplemental Figure 13

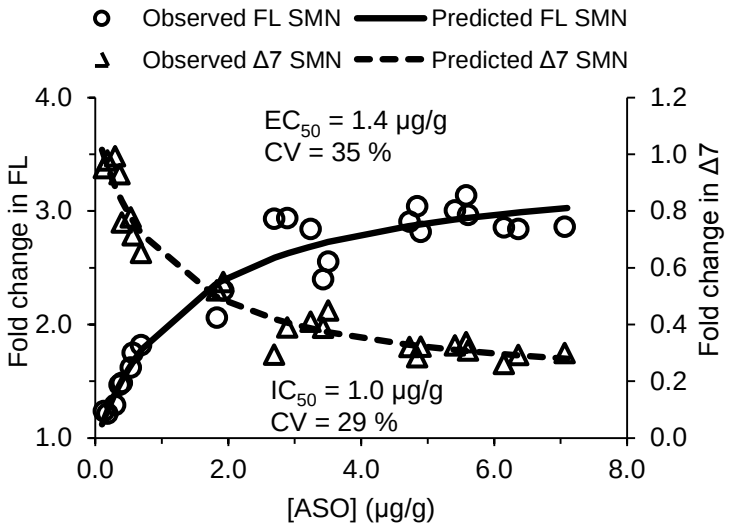

Supplemental Figure 14

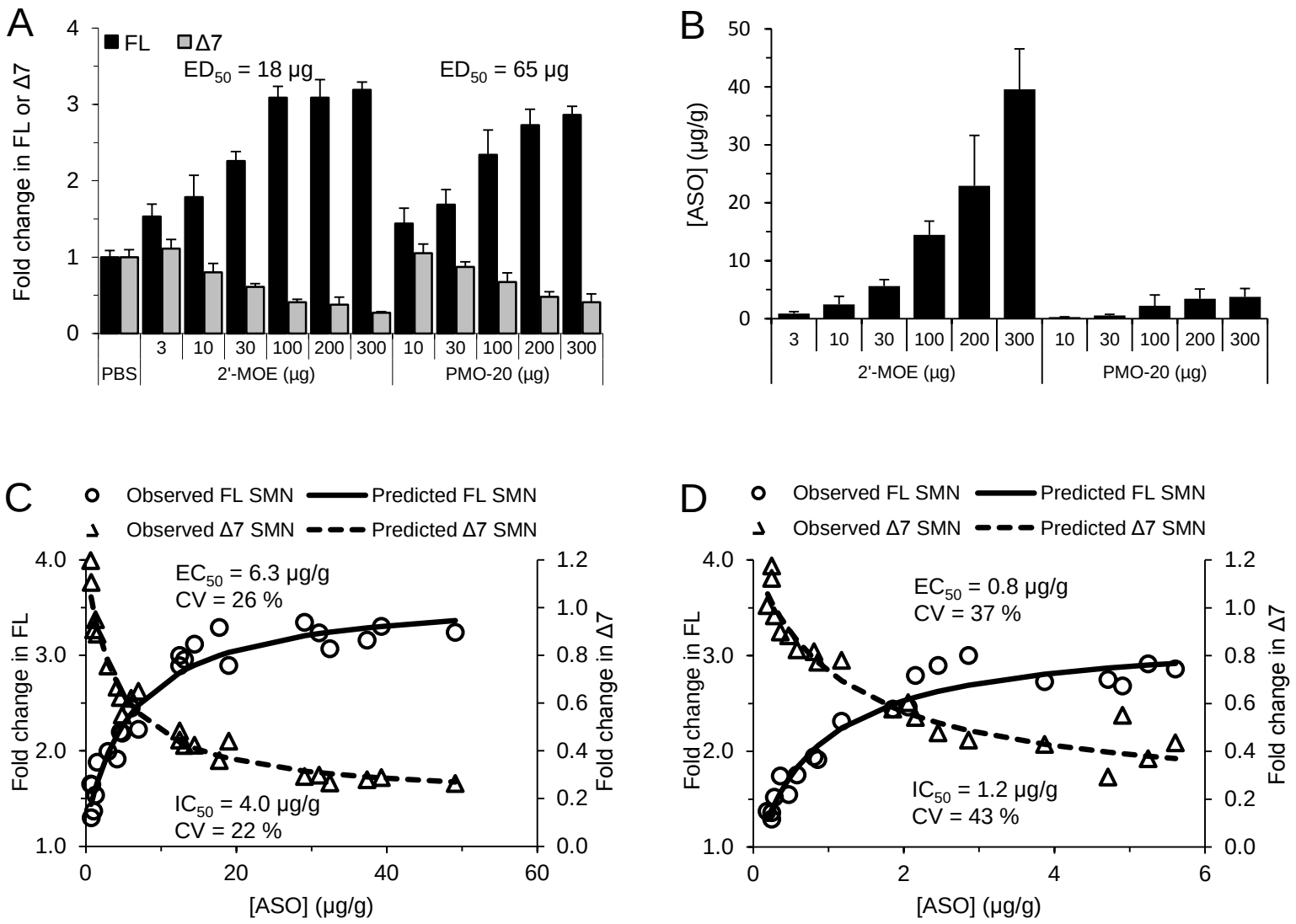

Supplemental Figure 15

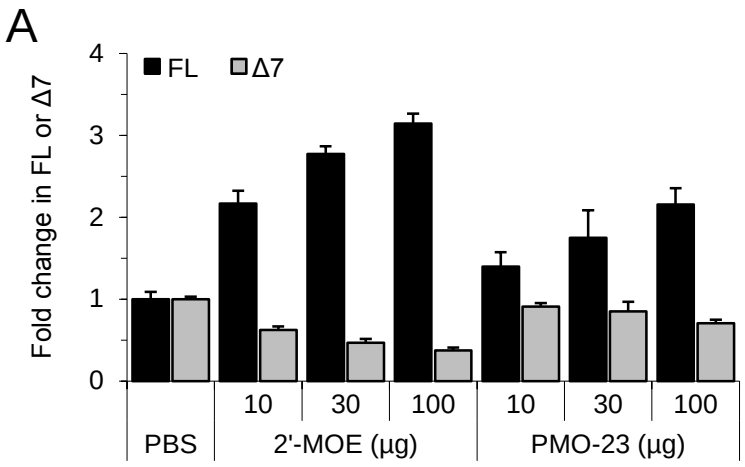

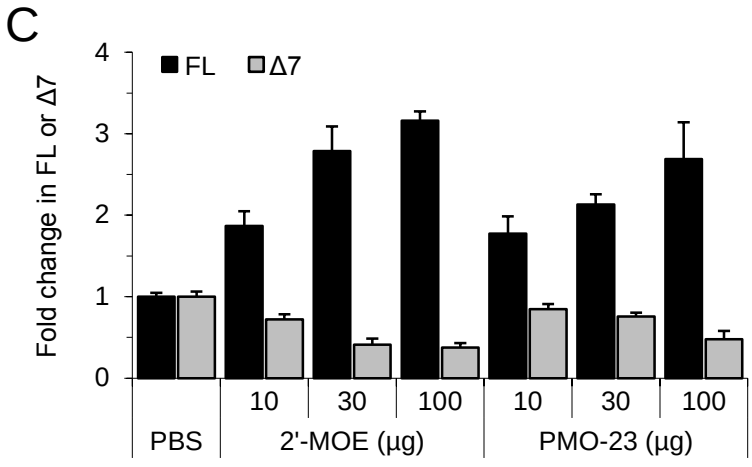

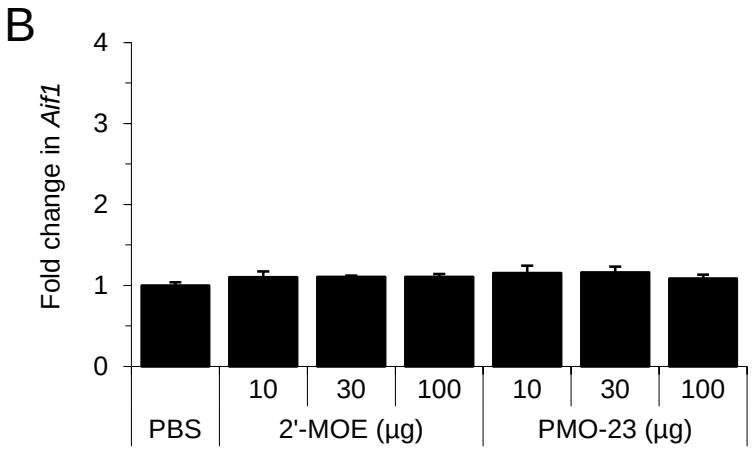

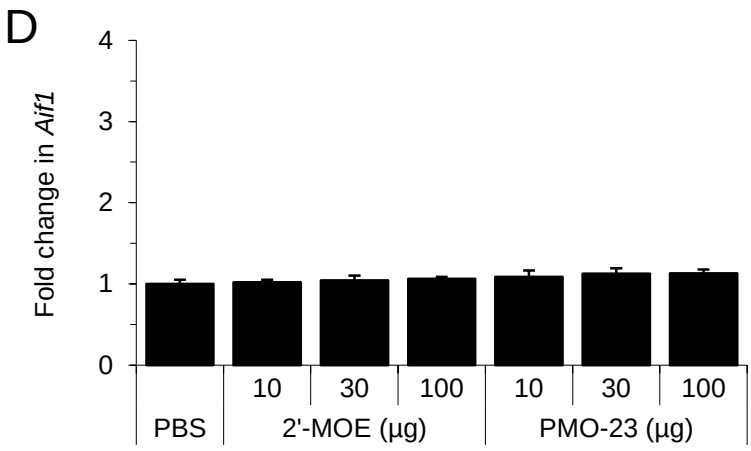

Supplemental Figure 16

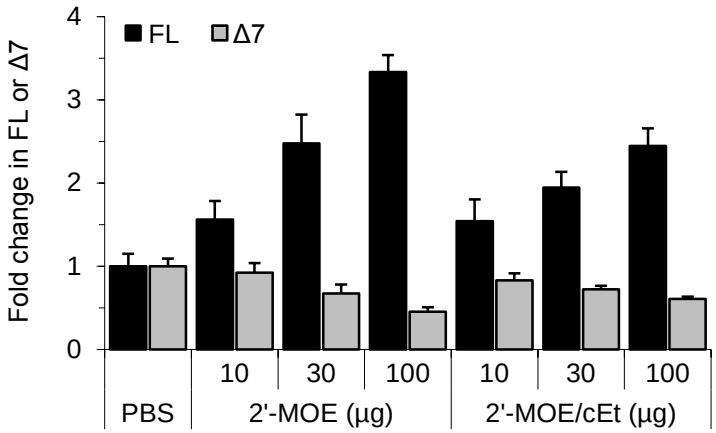

Supplemental Figure 17

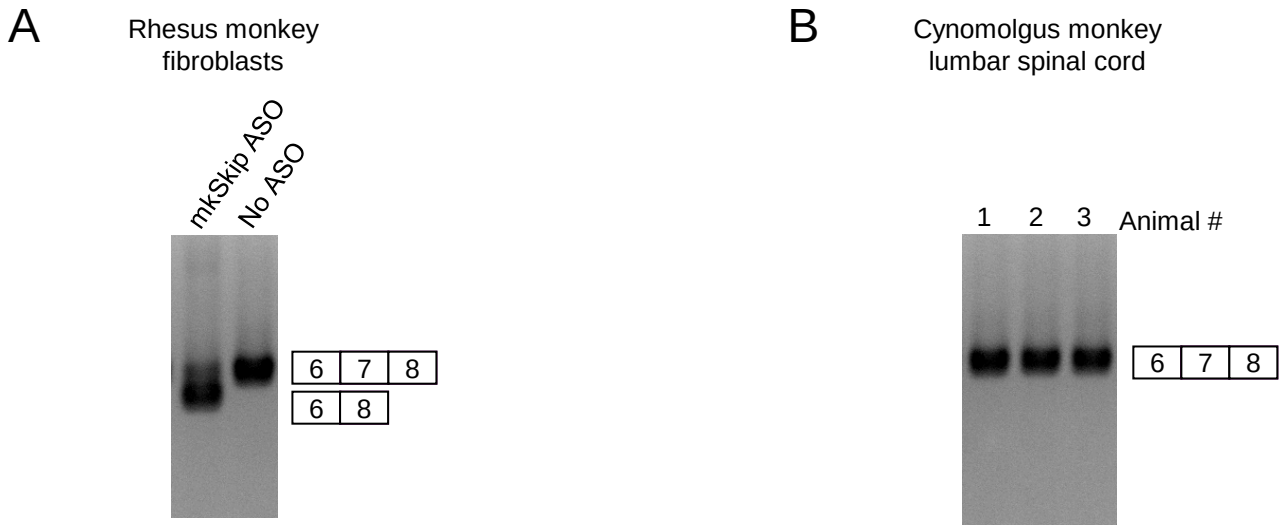

Supplemental Table 1

Name	Chemistry Notation (5'-3')
ISIS 396443	Tes mCes Aes mCes Tes Tes Tes mCes Aes Tes Aes Aes Tes Ges mCes Tes Ges Ge
2'-OMe ASO	Ams Ums Ums Cms Ams Cms Ums Ums Ums Cms Ams Ums Ams Ams Ums Gms Cms Ums Gms Gm
PMO-20 ASO	Axx Txx Txx Cxx Axx Cxx Txx Txx Txx Cxx Axx Txx Axx Axx Txx Gxx Cxx Txx Gxx Gx
PMO-23 ASO	Axx Axx Gxx Axx Txx Txx Cxx Axx Cxx Txx Txx Txx Cxx Axx Txx Axx Axx Txx Gxx Cxx Txx Gxx Gx
2'-MOE/cEt ASO	Uks mCes Aes Cks Tes Tes Uks mCes Aes Uks Aes Aes Uks Ges mCes Uks Ges Gk
mkSkip ASO	Aes mCes Tes Tes Aes mCes Tes mCes mCes Tes Tes Aes Aes Tes Tes Tes Aes Aes Ges Ge

Legend

Sugar name	Code		Heterocycle name	Code		Linker name	Code
2'-*O*-methoxyethyl ribose	e		Adenine	A		Phosphorthioate ester	s
2'-*O*-methylribose	m		Cytosine	C		Phosphorodiamidate	x
Morpholino	x		Thymine	T			
(S)-cEt	k		5-methylcytosine	mC			
			Guanine	G			
			Uracil	U			

Supplemental Table 2

Name	DNA Sequence (5'-3')	Citation
SMN2+7. F	GCTGATGCTTTGGGAAGTATGTTA	Hua et al., G&D 2010
SMN2+7.R	CACCTTCCTTCTTTTTGATTTTGTC	Hua et al., G&D 2010
SMN2+7.P	5'FAM/TACATGAGTGGCTATCATACT/3'MGBNFQ	Hua et al., G&D 2010
SMN2d7.F	TGGACCACCAATAATTCCCC	Hua et al., G&D 2010
SMN2d7.R	ATGCCAGCATTTCCATATAATAGCC	Hua et al., G&D 2010
SMN2d7.P	5'FAM/TCCAGATTCTCTTGATGATG/3'MGBNFQ	Hua et al., G&D 2010
SMNtot.F	CAGGAGGATTCCGTGCTGTT	
SMNtot.R	CAGTGCTGTATCATCCCAAATGTC	
SMNtot.P	5'FAM/ACAGGCCAGAGCGAT/3'MGBNFQ	
mAIF1.F	TGGTCCCCCAGCCAAGA	Hua et al., G&D 2010
mAIF1.R	CCCACCGTGTGACATCCA	Hua et al., G&D 2010
mAIF1.P	5'FAM/AGCTATCTCCGAGCTGCCCTGATTGG/3'TAMRA	Hua et al., G&D 2010
mGAPDH.F	GGCAAATTCAACGGCACAGT	Rigo et al., NCB 2012
mGAPDH.R	GGGTCTCGCTCCTGGAAGAT	Rigo et al., NCB 2012
mGAPDH.P	5'FAM/AAGGCCGAGAATGGGAAGCTTGTCATC/3'TAMRA	Rigo et al., NCB 2012
hGAPDH.F	GAAGGTGAAGGTCGGAGTC	Rigo et al., NCB 2012
hGAPDH.R	GAAGATGGTGATGGGATTTC	Rigo et al., NCB 2012
hGAPDH.P	5'FAM/CAAGCTTCCCGTTCTCAGCC/3'TAMRA	Rigo et al., NCB 2012
Oligo(dT)	TTTTTTTTTTTTTTTTT	
E4-33to55-F	AAGTGAGAACTCCAGGTCTCCTG	Hua et al., AJHG 2008
E8-15to36-R	GTGGTGTCATTTAGTGCTGCTC	Hua et al., AJHG 2008
mkSMN.F	ACATGAGTGGCTATCACACTGGCT	
mkSMN.R	ACAATGAACAGCCATGTCCACCAG	

SUPPLEMENTAL MATERIALS AND METHODS

Cell transfection. For Supplemental Fig. 11A, SMA patient fibroblasts (Coriel; GM03813) in a 96-well plate were transfected with increasing concentrations of ASO in Opti-MEM (Invitrogen) containing 1.5 μl/ml Cytofectin (Genlantis). 4 h later, the transfection medium was replaced with complete medium consisting of DMEM (Invitrogen) supplemented with 10% (v/v) FBS (Invitrogen). Incubation proceeded for another 20 h. For Supplemental Figs. 11B, C SMA patient fibroblasts in complete medium were added to a 96-well electroporation plate that contained ASOs at the required concentration. Cells were electroporated at 145 V using a BTX HT 200 plate handler and a BTX ECM 830 Electroporation Generator (Harvard Apparatus). Cells were then transferred to a 96-well plate that contained 1× penicillin/streptomycin (Invitrogen) and incubated for 24 hr. For Supplemental Fig. 17A, rhesus monkey fibroblasts DBSFRhL2 (ATCC; CL160) in a 6-well plate were transfected with 30 nM ASO using Cytofectin, as above.

Melting temperature measurements. Performed as previously described (Kawasaki et al., 1993).

SUPPLEMENTAL REFERENCES

Hua Y, Sahashi K, Hung G, Rigo F, Passini MA, Bennett CF and Krainer AR (2010) Antisense correction of SMN2 splicing in the CNS rescues necrosis in a type III SMA mouse model. *Genes Dev* **24**:1634-1644.

Kawasaki AM, Casper MD, Freier SM, Lesnik EA, Zounes MC, Cummins LL, Gonzalez C and Cook PD (1993) Uniformly modified 2'-deoxy-2'-fluoro phosphorothioate oligonucleotides as nuclease-resistant antisense compounds with high affinity and specificity for RNA targets. *J Med Chem* **36**:831-841.